

Identifying drug targets in tissues and whole blood with thermal-shift profiling

Jessica Perrin^{1,3}, Thilo Werner^{1,3}, Nils Kurzawa^{1,2,3}, Anna Rutkowska¹, Dorothee D. Childs², Mathias Kalxdorf¹, Daniel Poeckel¹, Eugenia Stonehouse¹, Katrin Strohmer¹, Bianca Heller¹, Douglas W. Thomson¹, Jana Krause¹, Isabelle Becher^{1,2}, H. Christian Eberl¹, Johanna Vappiani¹, Daniel C. Sevin¹, Christina E. Rau¹, Holger Franken¹, Wolfgang Huber², Maria Faelth-Savitski¹, Mikhail M. Savitski^{2*}, Marcus Bantscheff^{1*} and Giovanna Bergamini^{1*}

Monitoring drug–target interactions with methods such as the cellular thermal-shift assay (CETSA) is well established for simple cell systems but remains challenging in vivo. Here we introduce tissue thermal proteome profiling (tissue-TPP), which measures binding of small-molecule drugs to proteins in tissue samples from drug-treated animals by detecting changes in protein thermal stability using quantitative mass spectrometry. We report organ-specific, proteome-wide thermal stability maps and derive target profiles of the non-covalent histone deacetylase inhibitor panobinostat in rat liver, lung, kidney and spleen and of the B-Raf inhibitor vemurafenib in mouse testis. In addition, we devised blood-CETSA and blood-TPP and applied it to measure target and off-target engagement of panobinostat and the BET family inhibitor JQ1 directly in whole blood. Blood-TPP analysis of panobinostat confirmed its binding to known targets and also revealed thermal stabilization of the zinc-finger transcription factor ZNF512. These methods will help to elucidate the mechanisms of drug action in vivo.

TPP determines thermal stability across the proteome by measuring the soluble fractions of proteins upon heating cells and lysates to a range of temperatures. It also enables the proteome-wide assessment of drug–protein interactions by combining quantitative mass spectrometry¹ with CETSA^{2–4}. The CETSA methodology has recently been applied to tissues for detecting thermal stability changes of individual drug targets upon in vivo dosing^{2,5}; however, a strategy for the assessment of proteome-wide thermal stability and compound-selectivity profiling in vivo has been lacking. The ability to translate target and off-target engagement measurements from in vitro systems to in vivo studies is critical for predicting not only efficacy but also adverse reactions⁶.

Here we report a TPP-based method, tissue-TPP, to assess thermal stability across tissue proteomes and to study the engagement of targets and off-targets in organs of animals dosed with the non-covalent small-molecule histone deacetylase (HDAC) inhibitor, panobinostat, taking advantage of the extensive in vitro characterization of its selectivity in biochemical and cell-based assays^{7,8}.

We first determined protein targets of panobinostat in extracts derived from tissues and compared this profile to those derived from cell lines using a crude-extract protocol¹. In this lysis strategy, cells are broken up mechanically in the absence of detergent

and only after heating proteins are extracted with a mild detergent (Supplementary Fig. 1), resulting in better solubilization of membrane-bound proteins. The percentage of membrane proteins detected in crude cell extracts following this protocol was fourfold higher than in detergent-free extracts (PBS extracts) and almost comparable to that in intact cells (Supplementary Fig. 2a and Supplementary Data 1). In line with previous reports, melting temperatures (T_m) measured in HepG2 cells and HepG2 crude extracts showed a correlation of $r=0.58$, an expected value owing to differences in concentration of cellular co-factors and the alteration of protein–protein interactions (Supplementary Fig. 2b). When comparing T_m values in crude extracts from rat kidney, liver, spleen and testis, high correlations were determined ($r=0.87–0.93$; Supplementary Fig. 2c and Supplementary Data 2).

We then performed two-dimensional (2D)-TPP³ experiments with panobinostat in crude extracts from mouse and rat liver tissues and from the HepG2 cell line obtaining similar target profiles across all extracts (Supplementary Fig. 3a,b, Supplementary Table 1 and Supplementary Data 3). Notably, the multipass membrane FADS1, which is localized to the membrane of the endoplasmic reticulum and has been previously reported to be stabilized in live cells and not detected in PBS extracts⁸, was stabilized in crude extracts and could now be identified as a direct target of panobinostat (Supplementary Fig. 3c,d). This data shows that crude extracts derived from animal tissues can be used to generate in vitro cross-species selectivity profiles of small molecules with TPP.

We then applied tissue-TPP to organ sections derived from a rat in vivo study with panobinostat. Before proceeding with the analysis of the dosed animals, we analyzed the thermal stability of tissue proteomes in the control animals. Three control rats were killed and tissue samples derived from liver, lung, kidney and spleen were directly incubated at different temperatures ranging from 37 °C to 64 °C. After mechanical tissue disruption with a bead-based procedure and addition of DNase and a mild detergent, the soluble protein fraction was analyzed by quantitative mass spectrometry resulting in a total of 11,032 proteins detected across all four organs (Supplementary Data 4 and Supplementary Fig. 4a). The resulting proteome-wide thermal-stability profiles showed similar T_m distributions and high pairwise correlations (Fig. 1a) irrespective of protein-expression levels in the different organs (Supplementary Fig. 4b,c). Interestingly, the thermal-stability profiles in organs were also very

¹Cellzome GmbH, GlaxoSmithKline, Heidelberg, Germany. ²Genome Biology Unit, European Molecular Biology Laboratory, Heidelberg, Germany.

³These authors contributed equally: Jessica Perrin, Thilo Werner, Nils Kurzawa. *e-mail: mikhail.savitski@embl.de; marcus.x.bantscheff@gsk.com; giovanna.2.bergamini@gsk.com

similar to that generated in the rat cell line RBL-2H3 (Fig. 1b,c, Supplementary Fig. 4d and Supplementary Data 2 and 4). Despite the high diversity in structure and density of the different organs, heating appeared to have homogeneously affected all samples, demonstrating the general applicability of thermal proteome profiling to tissues.

To carry out a deeper analysis of the proteome thermal stability across tissues, we used a non-parametric analysis of response curves⁹ (NPARC; *F*-statistic-based strategy) for detecting differential melting behaviors (Supplementary Data 5). Incomplete denaturation curves were included in the analysis and the number of tested proteins increased by 16–20% as compared to the number of proteins with a defined melting point (Supplementary Fig. 5a). A total of 4,110 melting curves could be fitted in liver, 3,411 in kidney, 3,703 in lung and 4,218 in spleen (Supplementary Data 6), 2,144 of those were overlapping in all four tissues (Supplementary Fig. 5b). While the overall thermal profiles were consistent across the different organs, significantly different thermal denaturation curves between any of the four organs were identified for 637 proteins ($P \leq 0.001$) which were enriched for Gene Ontology (GO) terms such as ‘fatty acid β -oxidation’ and ‘cellular modified amino acid metabolic process’ (Supplementary Tables 2 and 3, Supplementary Fig. 5c and Supplementary Data 7). Proteins involved in these biological processes showed higher thermal stabilities and expression levels in liver and kidney as compared to lung and spleen (Supplementary Figs. 5d,e and 6a), potentially reflecting the high capacity for fatty acid β -oxidation of hepatocytes and proximal tubules in the kidneys¹⁰ and the key role of kidney and liver in the synthesis and interorgan exchange of amino acids in the body¹¹. Of note, a comparative analysis of protein abundances and thermal stabilities showed no overall correlation between these two datasets suggesting that tissue-TPP could provide information on protein states beyond levels of protein expression (Supplementary Fig. 6b).

Several factors can explain altered thermal stability of a protein, including post-translational modifications and protein–protein interactions as previously shown in cell cultures^{12,13}; however, so far it has been unclear whether such changes could be also detected in vivo. When analyzing the signal transducers and activators of transcription (Stat) family proteins, we observed significant differences ($P \leq 0.001$) in thermal stability, in particular, lower melting points in liver as compared to the other organs (Fig. 1d and Supplementary Fig. 7a). As Stat signaling is also regulated by tyrosine phosphorylation and a role in proliferation has been reported in hepatocytes¹⁴, we speculated that the observed stability changes may reflect, at least in part, differences in the phosphorylation state. Indeed, in comparison to kidney, we detected a higher proportion of phosphorylated Stat5 (pStat5) in liver (Fig. 1e), which showed lower melting temperature than the total Stat5 pool (Fig. 1f and Supplementary Fig. 7b).

We also analyzed the melting behavior of protein complexes in different organs using statistical methods previously reported for cultured and primary cells^{13,15,16} (Supplementary Fig. 8a,b and Supplementary Data 8 and 9). Across all tissues, stabilities of 57 protein complexes, either of the whole complex or of individual subunits, could be compared on the basis of melting points of their subunits (Supplementary Figs. 8c and 9a). Among those, the proteasome complex showed consistently higher thermal stability in the 20S proteasomal core subunits than the 19S subunit (Supplementary Fig. 9b). Differential thermal behavior was observed for Psmd4 and Psmd9, which was recently identified as a chaperone involved in proteasome assembly, but not a constitutive member of the assembled proteasome complex¹⁷. Interestingly, the subunit Psmd5 showed simultaneous melting with the other 19S components exclusively in kidney, suggesting specific regulation of the 19S complex in this organ. Also, the H^+ -transporting V-type ATPase, which is known to be required in kidney for deacidification of the blood¹⁸, showed a significantly higher median melting point specifically in this organ (Supplementary Data 8). Detailed comparison of the individual complex subunits revealed that along with an overall increase in thermal stability of the V1 subcomplex members, the melting point of the C subunit of V1 (v1c1) was significantly increased in kidney as compared to the other tissues (Fig. 1g). This would suggest the presence of a higher population of fully assembled complexes in kidney as the C subunit is known to dissociate from V1 upon detachment of V1 from V0, providing a rationale for the higher thermal stability measured for the complex in this organ¹⁹ (Fig. 1g).

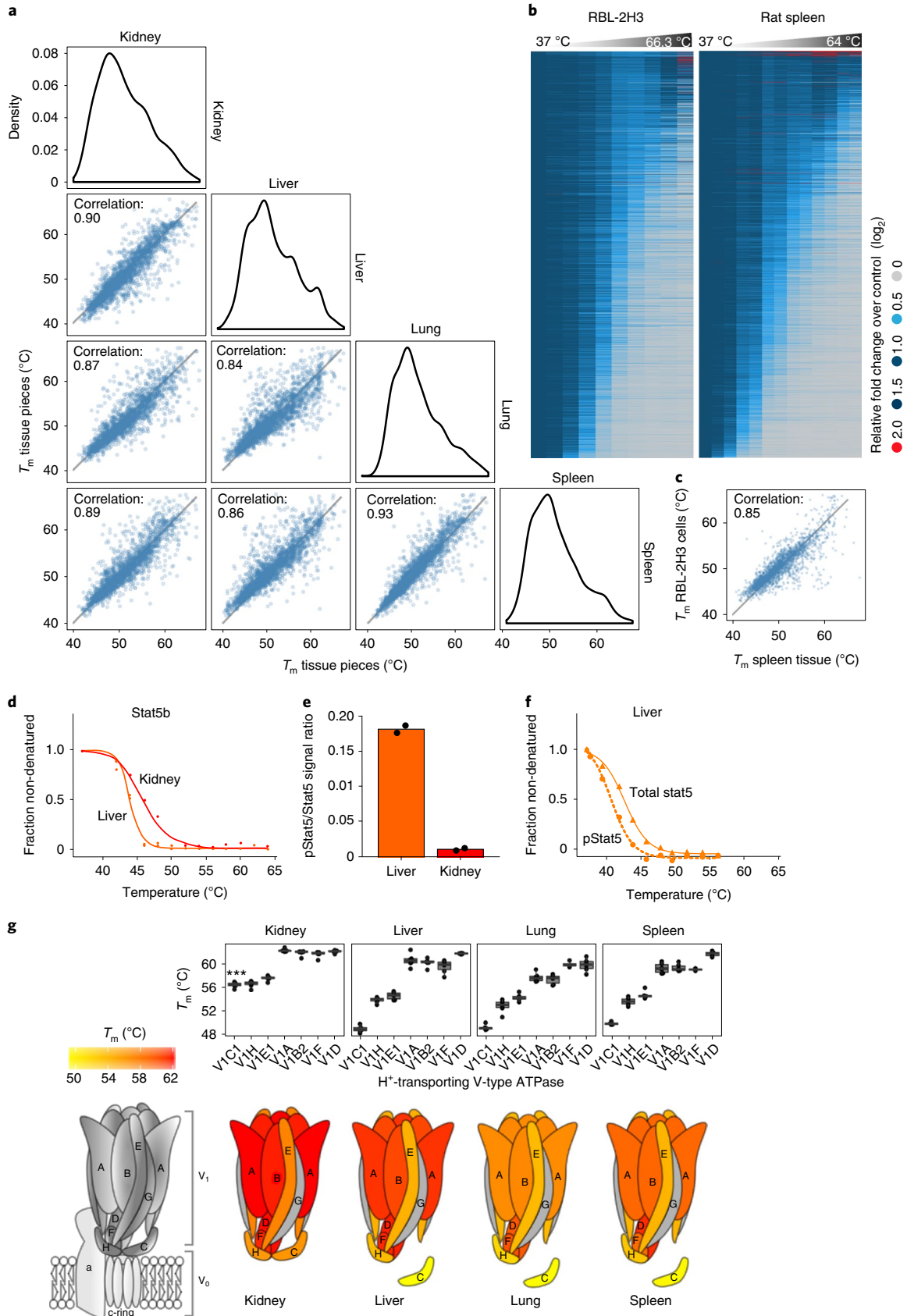
This data suggests that tissue-TPP, by reflecting protein post-translational modifications as well as protein–protein interactions, could be potentially used to monitor physiological processes in different organs in vivo.

We then analyzed tissue samples derived from three rats administered intravenously with 10 mg kg⁻¹ panobinostat and killed 90 minutes post-dose (Fig. 2a and Supplementary Fig. 1a). Following quantitative mass spectrometry analysis (Supplementary Fig. 10a and Supplementary Data 4 and 10), significant stabilization of Hdac1, Hdac2 and Ttc38 was observed in all analyzed tissues as shown for spleen in Fig. 2b and liver, kidney and lung in Supplementary Fig. 10b. Hdac6 was stabilized in both lung and spleen, while stabilization of Fads1, could be observed exclusively in lung. The different off-target profiles obtained across tissues reflected heterogeneous levels of protein expression and of drug exposure (Supplementary Data 11). Hdac1, Hdac2 and Ttc38 were less stabilized in liver where the lowest concentrations of free panobinostat were measured (Supplementary Fig. 10c)—in agreement with previous in vivo studies reporting the rapid metabolism of this drug in rats²⁰. In addition, we detected stabilization of dehydrogenase–reductase SDR family member 1, Dhrl1, which was not observed in any tissue

Fig. 1 | Analysis of proteome thermal stability in tissues and cell lines. a, Scatter plots and density plots of protein T_m in rat tissue pieces. In the scatter plots, the mean T_m ($n=3$) of robustly quantified proteins (blue dots) are compared pairwise in the indicated rat tissues. The correlation coefficient represents Pearson's ρ . Density plots illustrate the T_m values distribution over temperature. **b**, Heat map of protein thermal stabilities in live RBL-2H3 cells and rat spleen. The median relative abundance across replicates (RBL-2H3, $n=2$; spleen samples, $n=6$) at the indicated temperature is shown for each protein as fold change relative to the lowest measured temperature (37 °C). The 1,739 proteins robustly quantified in both sample types are plotted in the same order. **c**, Scatter plots of protein T_m values in RBL-2H3 cells and rat spleen. Blue dots represent the mean T_m of robustly quantified proteins (RBL-2H3, $n=2$; spleen samples, $n=3$). The correlation coefficient represents Pearson's ρ . **d**, Stat5b melting curves in rat kidney (red line, $T_m = 46$ °C) and liver (orange line, $T_m = 44$ °C) samples. **e**, Relative signal ratio of pStat5a/b (Ser726 and Ser731) to total Stat5b in liver (orange bar) and kidney (red bar) samples by immunoblot (mean of two samples with data points overlaid). **f**, Melting curve of pStat5a/b ($T_m = 41$ °C) and total Stat5b ($T_m = 43$ °C) in rat liver samples by immunoblot (mean of two samples). **g**, Thermal stabilities of the V-type ATPase subunits in rat tissue samples. Top, box plots of T_m values of the different subunits of the V1 complex across tissues ($n=6$). The significance levels were tested by two-sided Welch's *t* tests for each subunit in kidney versus any other tissue; *** $P < 0.001$. Kidney versus liver, $P = 3.8 \times 10^{-10}$; kidney versus spleen, $P = 2.4 \times 10^{-9}$; and kidney versus lung, $P = 4.2 \times 10^{-11}$. The center line in box plots is the median, the bounds of the boxes are the interquartile range (IQR) and the whiskers correspond to the highest or lowest respective value or if the lowest or highest value was an outlier ($>1.5 \times$ IQR from the bounds of the boxes) it is exactly $1.5 \times$ IQR. Bottom, T_m values of the V-type ATPase are mapped onto its schematic representation and visualized as color gradients.

crude extracts or in experiments with cell lines. To further investigate compound effects in tissue, we optimized a model in which live tissue slices can be incubated *ex vivo* (Fig. 2a, Supplementary Fig.

1a). In agreement with the *in vivo* study, we detected in rat spleen slices treated with panobinostat stabilization of Dhrrs1 (Fig. 2c, Supplementary Data 12), as well as metabolism of the compound



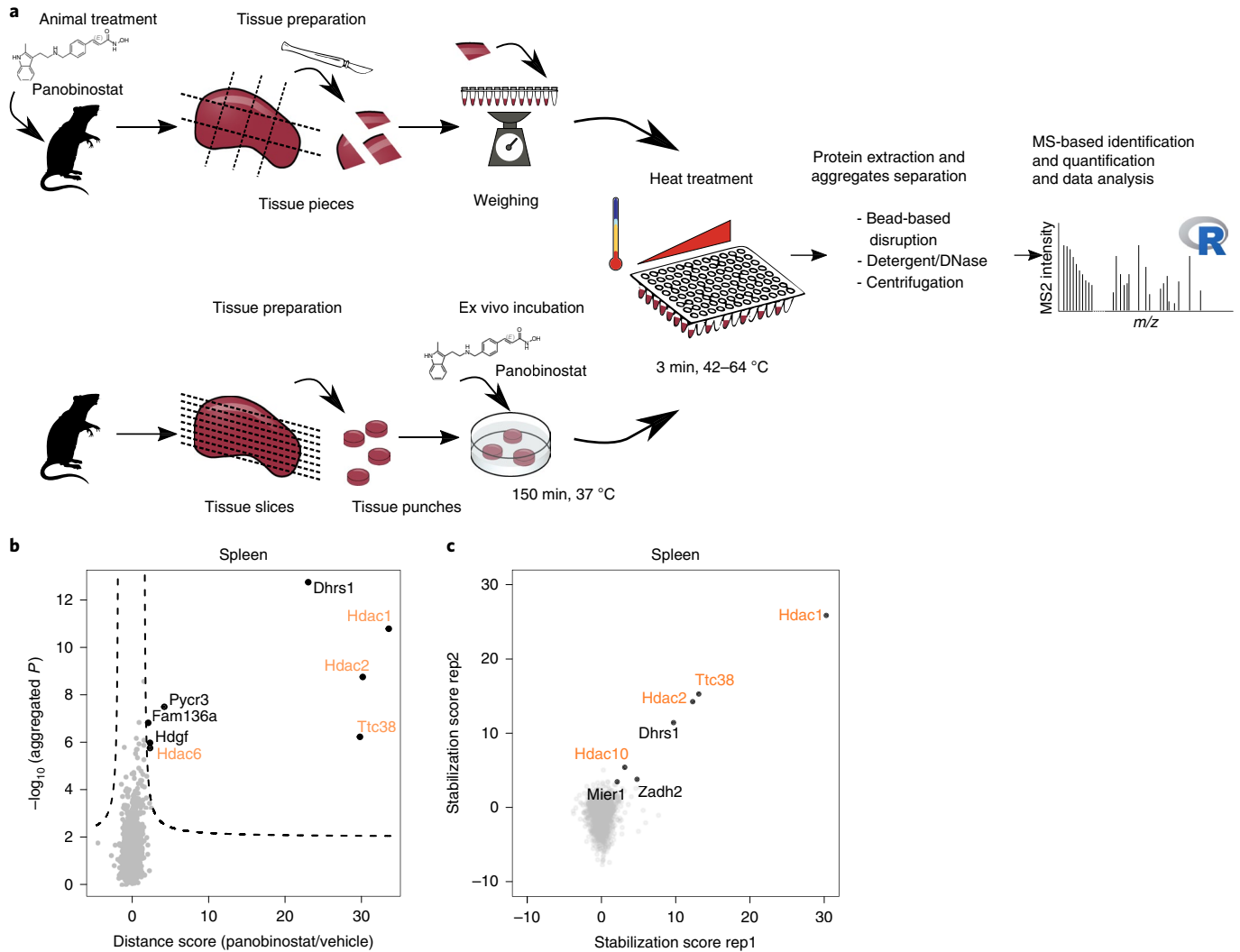


Fig. 2 | Panobinostat profiling in rat tissue in vivo and ex vivo. **a**, Tissue-TPP work flow for tissue pieces derived from in vivo dosed rats (upper panel). Rats were dosed intravenously with panobinostat or vehicle. One and a half hours after injection, the animals were killed and lung, spleen, liver and kidney were dissected into pieces. Samples were weighed and heat treated at temperatures from 42 to 64 °C for 3 min in buffer. After one freeze–thaw cycle, tissue samples were disrupted using ceramic beads and incubated with detergent and DNase for 60 min at 4 °C. The soluble proteins were separated by centrifugation, identified and analyzed by LC–MS/MS. Work flow for ex vivo tissue-TPP in rat spleen punches (lower panel). Punches generated from precision-cut slices (thickness 500 μ m, diameter 4 mm) from rat spleen were treated with panobinostat (50, 5, 0.5 and 0.05 μ M) for 150 min at 37 °C and 5% CO₂. After heat treatment, the analysis was performed as for the in vivo samples. **b**, Volcano plot showing protein targets stabilized in rat spleen following in vivo administration of panobinostat (10 mg kg⁻¹). Aggregated P values ($-\log_{10}$ transformed) and distance scores (\log_2 ratios aggregated across temperatures) of proteins quantified in spleens of panobinostat-dosed ($n=3$) versus vehicle-dosed ($n=3$) rats are displayed. The ratio-based approach used for the analysis included two-sided Student t tests for ratios between treatment and control groups obtained at each temperature, aggregation of retrieved P values per protein by Brown's method and multiple testing adjustment by the method of Benjamini–Hochberg (BH). Black dots, significantly affected proteins after BH correction; light gray dots, proteins that were not significantly affected; previously described targets of panobinostat⁸ are labeled in orange. **c**, Scatter plot of protein targets of panobinostat following ex vivo incubation in spleen tissue punches. Stabilization scores were displayed for two replicate 2D-TPP experiments (rep1, x axis; rep2, y axis). The stabilization score is a measure of monotonously increasing or decreasing protein thermal stability in response to increasing treatment concentrations (50, 5, 0.5 and 0.05 μ M) across different temperatures. Highlighted proteins were found as hits in both replicates according to the criteria described in ref. ⁸, previously described targets of panobinostat⁸ are labeled in orange.

(Supplementary Fig. 11, Supplementary Data 13–17). Overall, these findings indicate that stabilization of Dhrs1 can only be observed in metabolically active live tissue and might be due to a downstream cellular event since it does not result from direct binding of panobinostat. In addition to stabilization of the known targets Hdac1, Hdac2, Hdac10 and Ttc38 (Fig. 2c and Supplementary Data 12), Mier1, a known Hdac1/2 interactor⁷, was stabilized by panobinostat, further indicating the suitability of tissue-TPP for analyzing protein–protein interactions in organs.

To explore the applicability of tissue-TPP to other inhibitors, we incubated ex vivo the clinical drug vemurafenib²¹ in fragments of rat testis and demonstrated stabilization of targets and off-targets (Supplementary Fig. 12 and Supplementary Data 18). These data show the suitability of ex vivo tissue-TPP for investigating engagement of drug targets and off-targets in animal organs with the potential for future applications to human models. Importantly, in animals dosed with non-covalent small-molecule inhibitors, the engagement measured for the identified

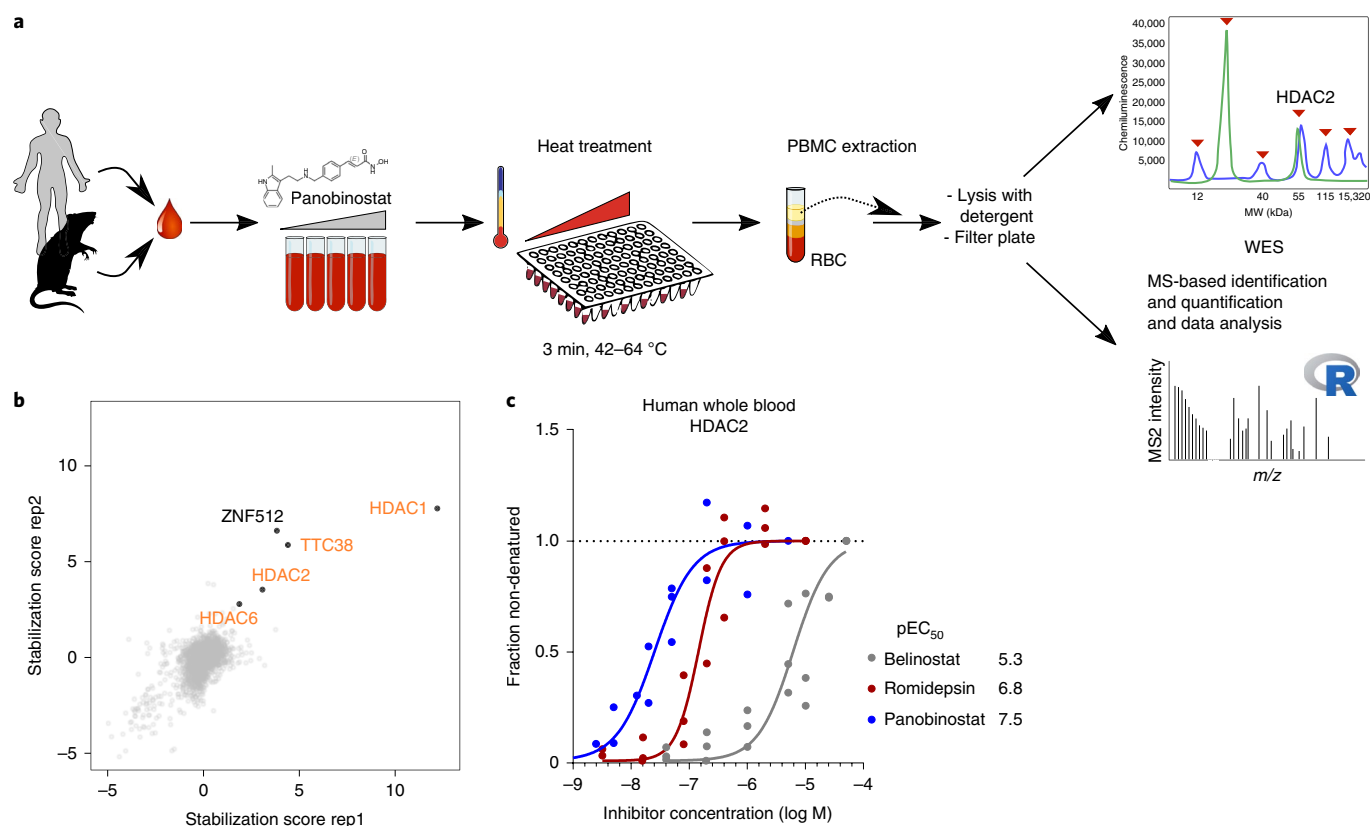


Fig. 3 | Thermal-shift assays in whole blood. **a**, Workflow of thermal-shift assays in whole blood. Fresh human or rat whole blood was treated ex vivo with panobinostat for 90 min at 37 °C and directly heated in PCR plates (3 min) with subsequent separation of PBMCs. After lysis and separation of aggregates, protein levels were measured in the soluble fraction by LC-MS/MS or WES, in blood-TPP or blood-CETSA, respectively. **b**, Scatter plot of protein targets of panobinostat following ex vivo incubation in human whole blood. Stabilization scores were displayed for two replicate 2D-TPP experiments (rep1, x axis; rep2, y axis). Highlighted proteins were found as hits in both replicates according to previously described criteria⁸; previously described targets of panobinostat⁸ are labeled in orange. **c**, Dose-dependent stabilization of HDAC2 by panobinostat, belinostat and romidepsin measured by blood-CETSA at 54 °C ($n=3$ donors); each data point is the mean of technical duplicates. Stabilization of HDAC2 in response to inhibitor treatment was measured relative to vehicle-treated control and fitted with saturation curves to determine the concentrations leading to half-maximal stabilization, pEC₅₀ ($-\log_{10}$ -transformed compound concentrations).

targets and off-targets by tissue-TPP correlates with drug exposure in tissue.

Next, we devised a thermal-stability-based method to measure target and off-target engagement directly in whole blood. Monitoring direct target engagement in vivo, together with efficacy biomarkers, enables the optimization of compound dosing regimens, which is essential to maximize efficacy as well as to avoid adverse effects. While in animal studies necropsies are typically accessible for analysis, in human studies blood samples are routinely analyzed and tissues biopsies are not always available.

We therefore optimized a procedure to prepare soluble proteins from heated whole-blood samples for analysis by quantitative mass spectrometry. This procedure, referred to as blood-TPP, includes heat treatment of whole blood, lysis of red blood cells and TPP analysis of purified peripheral blood mononuclear cells (PBMCs) (Fig. 3a). We observed similar thermal denaturation across the proteome of PBMCs purified from heated human whole blood and PBMCs heated after isolation from whole blood (Supplementary Fig. 13a) and found good correlation ($r=0.79$) of the melting points of the 2,054 proteins common to both datasets—of a total of 7,081 proteins identified in heated whole blood (Supplementary Fig. 13b). This data indicates the suitability of blood-TPP profiling offering the fundamental advantage with respect to TPP in purified cells of not introducing any additional dilution step before heat treatment, thus enabling a pharmacologically relevant measurement of target engagement.

We then investigated dose-dependent stabilization of panobinostat targets and off-targets in human blood samples subjected to temperatures from 44 to 54 °C. Mass-spectrometry analysis revealed dose-dependent stabilization of the targets HDAC1, HDAC2 and HDAC6 and the off-target TTC38 at similar concentrations observed in cell lines and tissue sections (Fig. 3b, Supplementary Fig. 14a and Supplementary Data 19). Whilst other off-targets such as PAH and FADS1/2 were not detected in the TPP analysis of blood samples owing to the low expression levels of these proteins, we observed dose-dependent stabilization of the zinc finger protein ZNF512. This specific effect on ZNF512 was never observed in the cell lines and tissues previously analyzed, most likely because of low levels of protein expression. To investigate the hypothesis that the hydroxamate moiety of panobinostat could bind the zinc ions of this transcription factor, we extended the analysis to other HDAC inhibitors and used HL-60 and THP-1 cell lines, which express high levels of this transcription factor. Panobinostat and SAHA, another hydroxamate-containing HDAC inhibitor, but not entinostat (which contains a different zinc-binding group, orthoamide), stabilized ZNF512, as well as the transcription factor ZNF148 (Supplementary Fig. 14b and Supplementary Data 20). These observations suggest that the previously unknown interactions with zinc-finger proteins may contribute to the differential pharmacological profiles of these HDAC inhibitors.

To explore the applicability of blood-TPP to small molecules other than HDAC inhibitors, we tested the bromodomain and extraterminal (BET) family inhibitor JQ1 (ref. 22) in human whole blood and measured stabilization of its known targets⁴ (Supplementary Fig. 14c and Supplementary Data 21).

Finally, to enable higher throughput for the blood assay we optimized an antibody-based read-out, referred to as blood-CETSA. Using these settings, we measured dose-dependent engagement of HDAC2 by panobinostat in human blood (pEC₅₀ 7.5, $-\log_{10}$ -transformed compound concentration leading to half-maximal stabilization of the target protein), as well as two additional marketed HDAC inhibitors, belinostat and romidepsin (Fig. 3c). The calculated pEC₅₀ values are in line with previous reports and compound ranking²³. In addition, we tested blood-CETSA on blood freshly derived from rats. In this setup, panobinostat induced dose-dependent stability changes of Hdac2, with a pEC₅₀ of 7.1 (Supplementary Fig. 14d), in agreement with the measurements in human blood. These data show how blood-CETSA could be used to monitor target engagement in preclinical studies enabling a direct cross-species translation from animals to humans. A quantitative measurement of the levels of target engaged after in vivo administration in preclinical and clinical studies could be achieved by the aid of a compound spiked-in control sample, which would enable normalization of the stabilization levels measured in each individual blood sample (Supplementary Fig. 14e).

Our study introduces tissue-TPP technology, which enables the hypothesis-free discovery of drug targets and off-targets in organ-derived crude extracts, in live tissue explants and following in vivo drug treatment. The tissue-specific profiles obtained for panobinostat highlight the importance of profiling compounds in tissues that are exposed to the drug in vivo to ultimately assess pharmacology as well as potential hazards associated with drug off-targets. Tissue-TPP also allows monitoring of processes at a molecular level directly in organs, enabling in vitro-to-in vivo translation of fundamental biological findings.

The blood-TPP and blood-CETSA approaches can readily identify drug targets and off-targets, and quantitatively measure target engagement in whole blood. Given the generally easier access to blood samples as compared to tissue biopsies, these approaches could be widely applied in clinical settings. In summary, we introduce and validate technologies broadly applicable both for fundamental research as well as in preclinical and clinical settings.

Online content

Any methods, additional references, Nature Research reporting summaries, source data, extended data, supplementary information, acknowledgements, peer review information; details of author contributions and competing interests; and statements of data and code availability are available at <https://doi.org/10.1038/s41587-019-0388-4>.

Received: 3 April 2019; Accepted: 6 December 2019;

Published online: 20 January 2020

References

- Bantscheff, M., Lemeer, S., Savitski, M. M. & Kuster, B. Quantitative mass spectrometry in proteomics: critical review update from 2007 to the present. *Anal. Bioanal. Chem.* **404**, 939–965 (2012).
- Molina, D. M. et al. Monitoring drug target engagement in cells and tissues using the cellular thermal shift assay. *Science* **341**, 84–87 (2013).
- Savitski, M. M. et al. Tracking cancer drugs in living cells by thermal profiling of the proteome. *Science* **346**, 1255784 (2014).
- Savitski, M. M. et al. Multiplexed proteome dynamics profiling reveals mechanisms controlling protein homeostasis. *Cell* **173**, 260–274 (2018).
- Ishii, T. et al. CETSA quantitatively verifies in vivo target engagement of novel RIPK1 inhibitors in various biospecimens. *Sci. Rep.* **7**, 13000 (2017).
- Morgan, P. et al. Can the flow of medicines be improved? Fundamental pharmacokinetic and pharmacological principles toward improving phase II survival. *Drug Discov. Today* **17**, 419–424 (2012).
- Bantscheff, M. et al. Chemoproteomics profiling of HDAC inhibitors reveals selective targeting of HDAC complexes. *Nat. Biotechnol.* **29**, 255–265 (2011).
- Becher, I. et al. Thermal profiling reveals phenylalanine hydroxylase as an off-target of panobinostat. *Nat. Chem. Biol.* **12**, 908–910 (2016).
- Childs, D. Non-parametric analysis of thermal proteome profiles reveals novel drug-binding proteins. *Mol. Cell Proteomics* **18**, 2506–2515 (2019).
- Bhargava, P. & Schnellmann, R. G. Mitochondrial energetics in the kidney. *Nat. Rev. Nephrol.* **13**, 629–646 (2017).
- van de Poll, M. C. G., Soeters, P. B., Deutz, N. E. P., Fearon, K. C. H. & Dejong, C. H. C. Renal metabolism of amino acids: its role in interorgan amino acid exchange. *Am. J. Clin. Nutr.* **79**, 185–197 (2004).
- Reinhard, F. B. M. et al. Thermal proteome profiling monitors ligand interactions with cellular membrane proteins. *Nat. Methods* **12**, 1129–1131 (2015).
- Tan, C. S. H. et al. Thermal proximity coaggregation for system-wide profiling of protein complex dynamics in cells. *Science* **359**, 1170–1177 (2018).
- Gao, B., Wang, H., Lafdil, F. & Feng, D. STAT proteins—key regulators of anti-viral responses, inflammation, and tumorigenesis in the liver. *J. Hepatol.* **57**, 430–441 (2012).
- Becher, I. et al. Pervasive protein thermal stability variation during the cell cycle. *Cell* **173**, 1495–1507 (2018).
- Mathieson, T. et al. Systematic analysis of protein turnover in primary cells. *Nat. Commun.* **9**, 689 (2018).
- Kaneko, T. et al. Assembly pathway of the mammalian proteasome base subcomplex is mediated by multiple specific chaperones. *Cell* **137**, 914–925 (2009).
- Al-Awqati, Q. Plasticity in epithelial polarity of renal intercalated cells: targeting of the H⁺-ATPase and band 3. *Am. J. Physiol.* **270**, C1571–C1580 (1996).
- Kane, P. M. Disassembly and reassembly of the yeast vacuolar H⁺-ATPase in vivo. *J. Biol. Chem.* **270**, 17025–17032 (1995).
- Assessment report Farydak, procedure No. EMA/H/C/003725/0000 (European Medicines Agency, 2015).
- Bollag, G. et al. Clinical efficacy of a RAF inhibitor needs broad target blockade in BRAF-mutant melanoma. *Nature* **467**, 596–599 (2010).
- Filippakopoulos, P. et al. Selective inhibition of BET bromodomains. *Nature* **468**, 1067–1073 (2010).
- Khan, N. et al. Determination of the class and isoform selectivity of small-molecule histone deacetylase inhibitors. *Biochem. J.* **409**, 581–589 (2008).

Publisher's note Springer Nature remains neutral with regard to jurisdictional claims in published maps and institutional affiliations.

© The Author(s), under exclusive licence to Springer Nature America, Inc. 2020

Methods

Reagents and cell culture. Reagents and media were purchased from Sigma unless otherwise stated. Compounds panobinostat (S1030), belinostat (S1085), romidepsin (S3020), vemurafenib (S1267), SAHA and entinostat were sourced from Selleckchem. JQ1 was sourced from Carboxynth (FC43273). RBL-2H3 cells and HL-60 cells were from DSMZ and HepG2 cells and THP1 cells were from ATCC. HepG2 cells were cultured in MEM (Gibco) containing 10% FBS (Gibco) supplemented with 1 mM sodium pyruvate (Gibco) and 1% non-essential amino acids (Gibco). RBL-2H3 cells were cultured in MEM containing 10% FBS and L-glutamine (2.0 mM; Gibco). HL-60 cells were cultured in RPMI (Gibco) 1640 medium containing 10% FBS. THP1 cells were cultured in RPMI supplemented with 10% FBS, 4.5 g l⁻¹ glucose, 10 mM HEPES and 1 mM sodium pyruvate. For all TPP experiments, PBS was supplemented with EDTA-free protease inhibitors (Roche, 11814389001) or additionally supplemented with a protease inhibitor mix (P8340). Anti-pSTAT5a/b (Ser726, Ser731) and anti-STAT5b were purchased from Invitrogen. Anti-HDAC2 was purchased from CST (5113) and from Abcam (Ab124974). Anti-SOD1 was purchased from Novus. Anti-Dhrs1 was purchased from Sigma (HPA000599). Detailed information on the antibodies, the experimental design and data analysis is included in the Life Sciences Reporting Summary.

Preparation of cells or tissue crude extracts. The crude cell extract was prepared as described⁴. HepG2 cells were dounce homogenized with 20 strokes in PBS supplemented with protease inhibitors. Rat livers (Heidelberg Pharma) and mouse livers (Charles River) were disrupted using ceramic beads (OMNI Bead Ruptor 24) in PBS supplemented with protease inhibitors. The cell or tissue suspensions were incubated for 1 h with benzonase (1 kU ml⁻¹, E1014) supplemented with 1.5 mM MgCl₂ (M1028). Protein concentration was determined by the Bradford assay (Bio-Rad, 500-0006) or the bicinchoninic acid assay (VWR, 733-1404). The preparation of PBS extract is described in ref. ⁸.

Preparation of tissue punches for live tissue compound incubation. Fresh spleen and testis from 10-week-old Wistar Han rats were provided by Heidelberg Pharma. Precision-cut slices of 500 μm thickness were prepared from fresh spleen using a Vibratome (VT1200S, Leica). Tissue punches of 4 mm diameter were generated using disposable biopsy punchers (pfm medical) and kept in cold medium (DMEM high glucose (Gibco)) during the procedure, supplemented with 10% FBS, penicillin–streptomycin 100 U ml⁻¹ (Gibco), L-glutamine (4.5 g l⁻¹), and 10 mM HEPES (Gibco).

The epididymis and envelope of the testes were removed before cutting the testis in the absence of medium into heterogeneously sized pieces using scalpels, on ice. Note, TPP-temperature range (TPP-TR) experiments refer to thermal-proteome profiles or thermal-stability profiles where the temperature is varied. 2D-TPP experiments refer to experiments where the temperature and the concentration of the test substance are varied.

An overview of all liquid chromatography–tandem mass spectrometry (LC–MS/MS) experiments is provided in Supplementary Data 22.

TPP-TR experiments. *TPP-TR experiments in cells.* TPP-TR was performed as described^{3,25}. In brief, RBL-2H3 and HepG2 cells were treated with vehicle (0.5% DMSO) for 90 min at 37 °C and 5% CO₂, then collected by trypsinization, aliquoted and heated for 3 min to a temperature range of 37 to 66.3 °C in PBS in a PCR plate. Igepal CA-630 (I3021) was added to a concentration of 0.8%, MgCl₂ (M1028) to 1.5 mM and benzonase to 1 kU ml⁻¹, and samples were incubated for 1 h at 4 °C. The aggregated proteins were separated by ultracentrifugation (20 min, 100,000g). Samples were further processed for LC–MS/MS analysis.

TPP-TR experiments in crude extracts of cells or tissues. Experiments were performed as described^{4,8}. Crude extracts at 2 mg ml⁻¹ protein concentration were incubated with vehicle (DMSO) for 15 min at 25 °C, then 12 wells of a PCR plate were filled with 100 μl (each) of each reaction. Samples were heated in parallel for 3 min to ten temperatures covering the range from 37 °C to 66.3 °C. Heat-treated samples were then rested for 3 min at room temperature. Igepal CA-630 (I3021) was added to a concentration of 0.8%, MgCl₂ (M1028) to 1.5 mM and benzonase to 1 kU ml⁻¹, and samples were incubated for 1 h at 4 °C. Aggregated proteins were separated by ultracentrifugation (20 min, 100,000g). Samples were further processed for LC–MS/MS analysis.

TPP-TR experiments in fragments of rat testis. Fragments of rat testis were added to a 96-well plate and the weight of the individual minced pieces was tracked using a scale. A volume of PBS supplemented with protease inhibitors equivalent to the volume of testis tissue (testis density: 1 g ml⁻¹ (ref. ²⁶)) was added to each well. Samples were heated in parallel for 3 min to ten temperatures covering the range from 37 °C to 66.3 °C. Heat-treated samples were rested for 3 min at room temperature and snap-frozen in liquid nitrogen. After thawing, the tissue pieces were disrupted by bead ruptor. Igepal CA-630 (I3021) was added to a concentration of 0.8%, MgCl₂ (M1028) to 1.5 mM and benzonase to 1 kU ml⁻¹, and samples were incubated for 1 h at 4 °C. Aggregated proteins were separated by ultracentrifugation (20 min, 100,000g). Samples were further processed for LC–MS/MS analysis.

TPP-TR experiments in human blood. After addition of protease inhibitors (1:200, P8340) fresh human heparinized blood samples (2 ml per condition) were distributed into a PCR plate and heat treated to ten temperatures covering the range from 37 °C to 62 °C for 3 min. PBMCs were retrieved by density centrifugation (Leucosep tubes, Greiner Bio-One, 163288) for 10 min at 1,000g at room temperature. After retrieval of PBMCs, contaminating erythrocytes were removed by incubating the PBMCs with red blood cell lysis buffer (Roche). The PBMCs were washed with PBS supplemented with protease inhibitors. PBMCs were resuspended and incubated for 1 h at 4 °C after supplementation of the buffer with Igepal CA-630 (final concentration 0.8%), benzonase (1 kU ml⁻¹) and 1.5 mM MgCl₂ at 4 °C. The lysates were then centrifuged for 3 min at 500g at 4 °C. The soluble protein fraction was retrieved by centrifugation of the supernatant through a 384-filter plate (Thermo Fisher Scientific, 10675743). Samples were further processed for LC–MS/MS analysis.

TPP-TR experiments in human PBMC. PBMCs were first purified from 45 ml of blood by density centrifugation (Leucosep tubes, Greiner Bio-One, 163288) as described above without the red blood cell lysis step. The PBMCs were then resuspended in 400 μl of PBS supplemented with protease inhibitors and 20 μl aliquots were distributed into a PCR plate and heat treated for 3 min at the respective temperature (ten temperatures covering 37.6–66.9 °C). Heat-treated samples were then rested for 3 min at room temperature and lysed as described above.

2D-TPP experiments. *2D-TPP in HepG2, HL-60 and THP1 cells.* Experiments were performed as described⁴. In brief, HepG2 cells were treated with vehicle (DMSO) or panobinostat (5, 1, 0.14 and 0.02 μM) for 90 min at 37 °C and 5% CO₂, and collected by centrifugation. Cells were resuspended in PBS and transferred to 96-well PCR plates and heated for 3 min to one of the 12 tested temperatures covering the range from 42 °C to 64 °C. After cell lysis (in presence of Igepal CA-630 (I3021) 0.8%, MgCl₂ (M1028) 1.5 mM and benzonase 1 kU ml⁻¹) the aggregated proteins were separated by ultracentrifugation (20 min, 100,000g). Samples were further processed for LC–MS/MS analysis.

Using similar conditions, THP1 cells and HL-60 cells were treated with vehicle (DMSO), SAHA (10, 2, 0.29 and 0.04 μM), entinostat (50, 10, 1.4 and 0.2 μM) or panobinostat (5, 1, 0.14 and 0.02 μM).

2D-TPP in crude cell or tissue extracts. Experiments were performed as described above with the following changes. Crude extracts were exposed to vehicle (DMSO) or panobinostat (5, 1, 0.14 and 0.02 μM) for 15 min at 25 °C. The samples were heated to 12 temperatures covering the range from 42 °C to 64 °C.

2D-TPP in live rat spleen tissues. Randomized spleen punch pieces (two per well) were distributed over 48-well plates containing 600 μl of DMEM high glucose (Gibco), supplemented with 10% FBS, 100 U ml⁻¹ penicillin–streptomycin (Gibco), 4.5 g l⁻¹ L-glutamine and 10 mM HEPES (Gibco). The spleen punch pieces were treated with panobinostat (50 μM, 5 μM, 0.5 μM and 0.05 μM) for 2.5 h at 37 °C and 5% CO₂. The punch pieces were then transferred to a 96-well PCR plate containing 100 μl of PBS supplemented with protease inhibitors and the respective panobinostat concentrations. Samples were heated in parallel for 3 min to one of the 12 tested temperatures covering the range from 42 °C to 64 °C and then processed as described above.

2D-TPP in rat testis live tissues. Fragments of testis were weighed into 96-well round-bottom cell culture plates containing 150 μl of medium. The testis pieces were treated with vemurafenib (40, 10, 2 and 0.4 μM) for 1.5 h at 37 °C and 5% CO₂, and was transferred to a 96-well PCR plate, centrifuged for a short period and the remaining medium was discarded. A volume of PBS (supplemented with protease inhibitors and the respective vemurafenib concentrations) equivalent to the volume of testis pieces (testis density, 1 g ml⁻¹ (ref. ²⁶)) was added to each well. The samples were processed as described above.

2D-TPP in human blood. Fresh human heparinized blood was treated with vehicle (DMSO), panobinostat (5 μM, 1 μM, 0.143 μM and 0.02 μM) or JQ1 (40, 10, 2 and 0.4 μM) for 1.5 h at 37 °C and 5% CO₂ (1.5–2 ml of blood per condition, depending on availability). After addition of protease inhibitors (1:200, #P8340), the blood was distributed into a PCR plate and heat treated for 3 min to five temperatures covering the range of 44 to 54 °C. PBMCs were retrieved by density centrifugation for 10 min at 1,000g at room temperature using SepMate-15 tubes (STEMCELL, 85420) and Lymphoprep density gradient medium (STEMCELL, 07811) combined with RosetteSe Human Granulocyte Depletion Cocktail (STEMCELL, 15624). The PBMCs were washed with PBS supplemented with protease inhibitors. The PBMCs were then lysed and processed as described above.

Tissue-TPP: in vivo rat panobinostat study. *In vivo study.* The rat in vivo study, including preparation of tissue pieces and heat treatment was performed by OncoDesign. Twelve 10-week-old male Han Wistar rats (CrI: WI(Han), Charles River) were distributed randomly into two groups of six rats. Group 1 was dosed intravenously (bolus) with 10 mg kg⁻¹ panobinostat and group 2 was dosed with vehicle (2% DMSO, 48% PEG 300 and 2% Tween 80 in water, pH 7). All rats were killed 90 min after dosing. The lung, liver, kidneys and spleen were collected from

each rat and cut with scalpels into two pieces. Half of the tissues were used for the tissue compound concentration measurement and the other half was used for tissue-TPP analysis.

Determination of tissue compound concentration. Lung, liver, kidney and spleen samples were homogenized in deionized water. Proteins were removed by precipitation using acetonitrile. The parent compound concentration in the supernatant was determined using LC-MS/MS analysis.

Heat treatment and lysis. The tissues were cut with scalpels into small pieces (20 mg to 50 mg per piece). Fourteen pieces per organ were transferred into PCR plates. Each piece of organ was weighed. Thirty microliters of cold PBS supplemented with protease inhibitors was added to each tissue before being heated for 3 min to 37 °C or 12 temperatures covering the range from 42 °C to 64 °C. The tissue pieces were then rested for 3 min at room temperature and snap-frozen in liquid nitrogen. After thawing, three volumes of PBS supplemented with protease inhibitors was added per volume of tissue (lung, liver, spleen and kidney tissue density ~1 g ml⁻¹ (ref. 26)), and the tissue pieces were disrupted by bead ruptor. Igepal CA-630 (I3021) was added to a concentration of 0.8% and MgCl₂ (M1028) to 1.5 mM, and samples were incubated for 1 h with benzonase (1 kU ml⁻¹) at 4 °C. Aggregated proteins were separated by ultracentrifugation (20 min, 100,000g). Samples were further processed for LC-MS/MS analysis.

Preparation of samples for LC-MS/MS analysis. Proteins were denatured using a sample based on lithium or sodium dodecyl sulfate (LDS or SDS, respectively) (NuPAGE LDS sample buffer, NP008 or 2× sample buffer (200 mM Tris-HCl (933313), 250 mM Trizma base (T1503), 20% glycerol (Merck, 1.04094), 4% SDS (Fluka, 5030) and 0.01% bromophenol blue (B8026)) and by incubating the samples for 30 min at 25 °C or 5 minutes at 95 °C. Proteins were partially separated by means of SDS gel electrophoresis or, alternatively, were directly processed (see below). Gel lanes were cut into three slices covering the entire separation range (~2 cm) and subjected to in-gel digestion with either LysC (Wako Chemicals) for 2 h and trypsin (Promega) overnight or trypsin only for 4 h. Peptide samples were labeled with TMT10 (Thermo Fisher Scientific) reagent. The labeling reaction was performed in 40 mM triethylammonium bicarbonate, pH 8.53, at 22 °C and quenched with glycine. Alternatively, proteins were digested following a modified solid-phase-enhanced sample preparation (SP3) protocol²⁷. In brief, proteins in 2% SDS were bound to paramagnetic beads (SeraMag Speed beads, GE Healthcare, 45152105050250, 651521050502) in filter plates (Multiscreen, Merck-Millipore, 10675743) and the plates were filled with 50% ethanol. Following washing of beads with four times 200 μl of 70% ethanol, beads were resuspended in trypsin and LysC in 0.1 M HEPES, pH 8.5 containing TCEP and chloracetamide and incubated at room temperature overnight and subjected to TMT labeling. Labeled peptide extracts were combined and samples from 2D-TPP, TPP-CCR (compound-concentration range) and TPP-TR experiments were subjected to additional fractionation on an UltiMate 3000 (Dionex) by reverse-phase chromatography at pH 12 on a 1-mm Xbridge column (Waters) and up to 24 fractions were collected. Depending on the analytical depth required, 8–24 fractions were analyzed by LC-MS/MS.

Liquid chromatography–tandem mass spectrometry. Samples were dried in vacuo and resuspended in 0.05% trifluoroacetic acid in water. Half of the sample was injected into an Ultimate3000 nanoRLSC (Dionex) coupled to a Q-Exactive (Thermo Fisher Scientific). Peptides were separated on custom-made 50 cm × 100 μm (ID) reverse-phase columns (Reprosil) at 55 °C. Gradient elution was performed from 2% acetonitrile to 40% acetonitrile in 0.1% formic acid and 3.5% DMSO over 65 min or 2 h. Samples were online injected into Q-Exactive or Orbitrap Fusion Lumos mass spectrometers. The Q-Exactive was operated in the data-dependent top 10 mode. Mass spectrometry spectra were acquired using a resolution of 70,000 and an ion target of 3 × 10⁶. Higher-energy collisional dissociation (HCD) scans were performed with 35% NCE at a resolution of 35,000 (at an *m/z* of 200) or 17,500 setting on a research-grade Q-Exactive Plus mass spectrometer using the phase-constrained spectrum deconvolution method²⁸; the ion-target setting was set to 2 × 10⁵ so as to avoid coalescence²⁹. The instruments were operated with Tune v.2.2 or v.2.3 and Xcalibur v.2.7 or v.3.0.63. The Orbitrap Fusion Lumos operated with a fixed cycle time of 3 s. Mass spectrometry spectra were acquired at a resolution of 60,000 and an ion target of 4 × 10⁵. HCD fragmentation was performed at 38% NCE at a resolution of 30,000 and an ion target 1 × 10⁵. The instrument was operated with Tune v.2.1.1565.23 and Xcalibur v.4.0.27.10. Information on which type of sample preparation (partial gel separation or SP3 protocol) and which instrument was used for MS/MS data acquisition can be retrieved in Supplementary Data 22.

Peptide and protein identification and quantification. Mascot v.2.4 (Matrix Science) was used for protein identification, a 10 p.p.m. mass tolerance for peptide precursors and 20-mDa (HCD) mass tolerance for fragment ions was selected. Carbamidomethylation of cysteine residues and TMT modification of lysine residues were selected as fixed modifications. Methionine oxidation, N-terminal acetylation of proteins and TMT modifications of peptide N termini were selected as variable modifications. The proteins were searched using Uniprot or Swissprot for human samples. The following criteria were used for protein identifications: (i)

for single spectrum-to-sequence assignments, we required this assignment to be the best match with a minimum Mascot score of 31 and a 10× difference over the next best assignment (using these criteria, the decoy search results indicated a <1% false-discovery rate); (ii) for multiple spectrum-to-sequence assignments and using the same parameters, the decoy search results indicate <0.1% FDR. Reporter ion intensities were read from the raw data and multiplied by ion accumulation times (measured in ms) to yield a measure proportional to the number of ions (this measure is referred to as ion area³⁰). Spectra matching to peptides were filtered according to the following criteria: mascot ion score >15; signal-to-background of the precursor ion >4; and signal-to-interference >0.5 (ref. 31). Fold changes were corrected for isotope purity and adjusted for interference caused by simultaneous elution near isobaric peaks as estimated by the signal-to-interference measure³⁰. Protein quantification values were calculated from individual spectra matching unique peptides using a sum-based bootstrap algorithm; 95% confidence intervals were calculated for all protein fold changes that were quantified with more than three spectra³⁰. An automatic outlier removal procedure was performed on proteins with at least five quantified PSMs (peptide-spectrum matches). In brief, each PSM and respective quantification values were sequentially excluded from the fold-change calculation; in cases where the confidence interval was then improved by at least 30%, the given quantification values were permanently excluded from further analyses.

Stat5a and Stat5b have very similar sequences. When both were identified, only peptides that were unique for one of the two genes were used for quantification, resulting in a lower number of quantified peptides for Stat5a and Stat5b.

Analysis of TPP-TR experiments. Experiments were analyzed as described²⁵. Following LC-MS/MS analysis, protein fold changes at each temperature were computed relative to the protein abundance at 37 °C. These fold changes represent the relative amount of non-denatured protein at the corresponding temperature. After a global normalization procedure³, melting curves were fitted to the fold changes of each individual protein according to the following equation:

$$f(T) = \frac{1 - \text{plateau}}{1 + e^{-\frac{(T-b)}{a}}} + \text{plateau} \quad (1)$$

where *T* is the temperature and *a*, *b* and plateau are constants. The *T_m* of the protein under the corresponding condition is given by the temperature at which the value of the melting curve is 0.5. Model fitting was performed by non-linear regression using the nls function in R, as described²⁵. *T_m* values were only reported if predicted to be located inside the measured temperature range.

Median *T_m* values were calculated and reported if the protein was quantified with at least two unique peptides in both replicates. *T_m* values were visualized in pairwise scatter plots (Fig. 1a,c, Supplementary Figs. 1c,d,3d and 10b), if they additionally showed a *T_m* difference between replicates smaller or equal to 2 °C and an average fitted plateau parameter of smaller or equal to 0.2.

Analysis of 2D-TPP experiments. Experiments were analyzed as described⁶. Each 2D-TPP experiment consisted of six TMT10 experiments (except the 2D-TPP experiments in whole blood which consisted of three TMT10 experiments), each containing the four compound concentrations and one vehicle control (at two consecutive temperatures). For each TMT10 experiment, the two vehicle conditions at the two selected temperatures were used as the reference for fold-change calculations for the two sets of four compound concentrations and the vehicle condition at the respective temperatures. The five different fold change values at each temperature condition were transformed to a range of between 0 and 1.

The following filtering criteria were used to consider a protein as stabilized in response to the compound treatment: proteins had to be identified by more than one unique peptide (q_{upm} > 1) in at least one of the experiments of the set. Proteins were required to be stabilized by the compound treatment at the maximum concentration by at least 50% (untransformed fold changes) as compared to the vehicle condition, in at least two adjacent temperature conditions.

A sigmoidal curve according to the following equation was fitted to derive pEC₅₀ values:

$$Y = \frac{1}{1 + 10^{(\log \text{EC}_{50} - x) \text{ slope}}} \quad (2)$$

Generation of scatter plots of 2D-TPP experiments. For generating the plots displayed in Fig. 2c and Supplementary Figs. 9a and 10e, a stabilization score δ was computed for each protein in each replicate with at least one measurement with q_{upm} > 1:

$$\delta = \begin{cases} \delta_{\text{stab.}}, \sum_{i=0}^c (r_i) \geq 0 \\ 0, \sum_{i=0}^c (r_i) \geq 0 \text{ and } \delta_{\text{stab.}} < 0 \text{ or } \sum_{i=0}^c (r_i) < 0 \text{ and } \delta_{\text{destab.}} > 0 \\ \delta_{\text{destab.}}, \sum_{i=0}^c (r_i) < 0 \end{cases} \quad (3)$$

where

$$\begin{aligned} \delta_{\text{stab.}} &= \sum_{i=0}^c \log_2(r_i) - \max_{j=1}^{c-1} (\log_2(r_j)), \delta_{\text{destab.}} \\ &= \sum_{i=0}^c \log_2(r_i) - \min_{j=1}^{c-1} (\log_2(r_j)) \end{aligned}$$

and where r_i are the relative fold changes at treatment condition i as compared to control and c is the number of concentrations.

The stabilization score is a measure of monotonously increasing or decreasing protein thermal stability in response to increasing treatment concentrations across different temperatures.

Stabilization scores from both replicates were plotted as scatter plots and detected targets passing the criteria above were labeled.

Analysis of in vivo rat panobinostat study. *Description of TMT10 sample set.* Each tissue type (lung, liver, spleen and kidney) was analyzed in a separate set of TMT10 experiments. Each TMT10 sample set contained five tissue extracts from one vehicle-treated rat and five tissue extracts from one panobinostat-treated rat, heated at five different temperatures (37°C and four additional temperatures; Supplementary Fig. 7a). Three TMT10 sample sets, when combined, enabled the generation of a full temperature gradient with 13 distinct temperatures per rat.

Preprocessing. Protein fold-changes were calculated relative to the 37°C vehicle-treated sample by dividing their sum ion areas. Vehicle-treated samples were normalized at each temperature as follows. First, proteins fulfilling the following criteria were selected for the calculation of the normalization factor: (i) quantified with at least three individual spectra matching unique peptides and at least two unique peptides; and (ii) a fold-change ≥ 0.2 relative to the 37°C-treated sample. The empirical distribution of the fold change was generated for each replicate and temperature. A normalization factor per temperature was calculated as the mean of the fold change at the respective distribution maximum in each replicate. All protein fold changes of vehicle-treated samples in the respective experiments were multiplied with the normalization factors.

The fold changes of the panobinostat-treated sample were normalized as described for vehicle-treated samples with the following changes: a normalization factor per temperature and replicate was calculated as the difference between the fold change at the distribution maximum of the panobinostat- and vehicle-treated groups. These normalization factors were then applied to all protein fold changes of the panobinostat-treated condition.

The normalized vehicle-treated and panobinostat-treated datasets were then combined. Protein fold changes of the panobinostat-treatment condition were scaled to the 37°C panobinostat-treated sample per protein.

Determination of T_m estimates for TPP-TR experiments with intact tissues pieces. Protein melting curves were fitted according to equation (1) per condition (vehicle and panobinostat-treatment) through one two or three data points per temperature where each data point reflected a biological replicate. A single T_m per protein and tissue was computed as the mean of the T_m determined from the vehicle curve and the panobinostat curve.

Statistical analysis of panobinostat-induced thermal stability effects: ratio-based approach. Proteins quantified in at least two replicate TMT10 experiments covering the same temperatures were included. If the average relative fold change in treatment or control was ≥ 0.4 at the highest temperature, the proteins were filtered out. If the median $R^2 < 0.8$ from the fitted melting curve in controls or treatment, the protein was filtered out.

For each protein and at each temperature, two parameters were calculated: the mean abundance ratio between treatment and control, and the significance of an abundance difference by left- and right-tailed one-sample t tests on the basis of \log_2 -transformed treatment to control ratios. If the protein relative fold change at a temperature was < 0.15 in the vehicle-treated and the panobinostat-treated condition, the \log_2 ratio at the specific temperature was removed. All P values were aggregated by the empirical Brown's method³² separately for the left-tailed test and the right-tailed test. For the covariance matrix calculation, the \log_2 ratios of each replicate and each P value was used. A protein abundance ratio was used as second effect size to evaluate if the panobinostat treatment had a significant effect. If the P value of the previously described t test on the \log_2 ratios was smaller than 0.05 at several consecutive temperatures, the average \log_2 ratios were summed. If several were recognized, the one with the highest summed ratio was selected (aggregated \log_2 ratio). If a protein showed no or only one P value < 0.05 , the average \log_2 ratio at the lowest P value was reported. Aggregated ratios were normalized to a distance score according to the following equation:

$$\text{Distance score} = \frac{x - \bar{x}}{S} \quad (4)$$

where x is the aggregated ratio of the respective protein, \bar{x} is the mean of aggregated ratios and S is the s.d. of aggregated ratios.

Proteins were regarded as significantly affected if they fulfilled the following criteria:

$$\text{if}(\Sigma r_{T_{VSC}} > s) \left\{ -\log_{10}(P) > \frac{1}{(\Sigma r_{T_{VSC}} - s)} + P \right\} \quad (5)$$

$$\text{if}(\Sigma r_{T_{VSC}} < -s) \left\{ -\log_{10}(P) > \frac{1}{(s - \Sigma r_{T_{VSC}})} + P \right\} \quad (6)$$

where $\Sigma r_{T_{VSC}}$ is the aggregated \log_2 ratio, s is the s.d. of the dataset defined as $10 \times \text{median s.d. of ratios between replicates}$ and P is the minimal accepted $-\log_{10}$ -transformed P value set to $P = 0.01$. Proteins that were significant after the Benjamini–Hochberg correction³³ were highlighted. The cutoff was set to 0.1. The Benjamini–Hochberg correction was calculated with a double amount of proteins, as two P values were calculated per temperature and protein.

Functional inference of tissue differences in protein melting. To compare melting curves between organs, we developed an approach using functional inference (D.C. et al., manuscript in preparation). The approach is based on fitting two competing models to the data. The null model states that the temperature response is explained by a smooth melting curve according to equation (1). The alternative model replaces this common function by organ-specific curves. To detect proteins with different melting curves between organs, we constructed an F statistic that quantified improvements in goodness-of-fit of the alternative model relative to the null model:

$$F_i = \frac{\text{RSS}_i^0 - \text{RSS}_i^1}{\text{RSS}_i^1} \cdot \frac{df_{i2}}{df_{i1}} \quad (7)$$

where RSS_i^0 is the sum of squared residuals of the null model fit to protein i , RSS_i^1 is the sum of squared residuals of the alternative model fit to protein i , df_{i1} is the degrees of freedom parameter of the numerator $\text{RSS}_i^0 - \text{RSS}_i^1$ and df_{i2} is the degrees of freedom parameter of the denominator RSS_i^1 .

The values of df_{i1} and df_{i2} could not be analytically derived owing to correlated and heteroscedastic residuals. To estimate the null distribution of F_i , we generated a null dataset by randomly permuting the tissue labels per protein without replacement. The F statistic numerator $\text{RSS}_i^0 - \text{RSS}_i^1$ and the denominator RSS_i^1 were recalculated on the basis of this null data. The distribution parameters were estimated by numerically fitting a χ^2 distribution separately to the values of $\text{RSS}_i^0 - \text{RSS}_i^1$ (to obtain df_{i1}) and of RSS_i^1 (to obtain df_{i2}) in R. A scaling parameter for the χ^2 distribution was calculated from the empirical distribution of the values of $\text{RSS}_i^0 - \text{RSS}_i^1$ (excluding values within the upper 5% quantile) in the label-permuted dataset according to the following equation:

$$\sigma_0^2 = \frac{\text{Var}(\text{RSS}^0 - \text{RSS}^1)}{2 \cdot \text{mean}(\text{RSS}^0 - \text{RSS}^1)} \quad (8)$$

All values of $\text{RSS}_i^0 - \text{RSS}_i^1$ and of RSS_i^1 that were obtained from the label-permuted dataset were divided by σ_0^2 before the numerical fit of the χ^2 distribution.

The estimated degrees of freedom were used to calculate F_i according to equation (8), with the numerator and denominator obtained from the original data. We computed P values by comparing each F_i to an F distribution with the estimated degrees of freedom. All P values were adjusted for multiple testing by the Benjamini–Hochberg correction³³.

Clustering. Proteins identified in all tissues and with an adjusted F test $P \leq 0.001$ in any of the cross-tissue comparisons were used for clustering. Clustering was done using complete linkage and Euclidian distance in Tibco Spotfire v.7.0.1.24. For the clustering in the heat map (Supplementary Fig. 4c) the median normalized area under the curve (AUC) ($\text{AUC}_i - \text{median}_{\text{all tissues}}$) per tissue was used to display the differences of protein melting behavior in the four tissues. For the clustering in the heat map (Supplementary Fig. 4f), the z -transformed MS1 intensities (Top3 quantification³⁴; at 37°C) of individual proteins were used to display the relative protein concentrations in the four tissues. GO enrichment was performed using the online enrichment tool Gorilla^{35,36} using all identified proteins as a background.

Analysis of thermal stability of proteins in complexes. Proteins were mapped to complexes using annotations comprising the databases CORUM^{37,38} and COMPLEAT³⁹ as previously compiled⁴⁰.

To assess whether differences in melting points of complex members were less than would be expected by chance, we used a strategy described previously for protein half-lives¹⁶, where the s.d. of melting points of complex members was compared to those computed from a permuted version of the same list.

To compare thermal stabilities of protein complexes across tissues, median melting points of protein complex members identified and characterized across all tissues were determined and compared.

To evaluate co-melting of complex members with potential interaction partners, we applied a previously suggested strategy¹³, where average Euclidean distances of fold changes at respective temperatures between two proteins of interest were compared with 10,000 random comparisons. This approach makes it possible to calculate P values, by comparing the Euclidean distance of a given protein pair with the distribution of randomly drawn comparisons.

Determination of Stat5 and pStat5 levels and T_m in rat tissues. Liver and kidneys were dissected from untreated 10-week-old Han Wistar rats (Heidelberg Pharma), cut into pieces of 30 to 60 mg and distributed over 96-well PCR plates. A volume of PBS supplemented with protease inhibitors equivalent to the volume of liver and kidney pieces was added to each well. Samples were heated in parallel for 3 min to temperatures covering the range from 37°C to 56.4°C. Heat-treated samples were

rested for 3 min at room temperature and disrupted by bead ruptor. Non-heat-treated tissue pieces were directly disrupted by bead ruptor. Igepal CA-630 (I3021) was added to a concentration of 0.8% and MgCl_2 (M1028) to 1.5 mM, and samples were incubated for 1 h with benzonase (1 kU ml^{-1}) at 4°C . Aggregated proteins were separated by ultracentrifugation (20 min, 100,000g) and denatured with an SDS-based sample buffer. Lysates were analyzed by immunoblot for pSTAT5a/b (Ser726, Ser731) (Invitrogen, PA5-36767) and total STAT5b (Invitrogen, 135300) signals in two biological replicates.

To derive pEC_{50} values, the fold change values were transformed to a range between 0 and 1. A sigmoidal curve was fitted using GraphPad Prism 7 to derive pEC_{50} values, according to equation (2).

Blood-CETSA experiments and detection of HDAC2 by Western Assay System.

Fresh rat or human heparinized blood was treated with different concentrations of panobinostat (5, 1, 0.2, 0.05, 0.0125 and 0.0025 μM), romidepsin (30, 10, 2, 0.4, 0.2, 0.08, 0.01 and 0.0032 μM), belinostat (50, 25, 10, 5, 1, 0.2 and 0.04 μM), or vehicle for 90 min at 37°C and 5% CO_2 (1.5–1.75 ml of blood per condition, depending on availability). After the addition of protease inhibitors (1:200, P8340), the blood was then distributed into a 96-well PCR plate and heat treated for 3 min to 54°C (human) and 53°C (rat blood). PBMCs were retrieved by density centrifugation (Leucosep tubes, Greiner Bio-One, 163288) for 10 min at 1,000g at room temperature. The PBMCs were then lysed and processed as described under 'TPP experiments in human blood'. The denatured samples were further diluted in Western Assay System (WES) buffer (Protein Simple, 042-195) and relative abundance of HDAC2 (CST 5113, human blood; Abcam Ab124974, rat blood) and SOD1 (Novus, NBP1-90186) were analyzed by capillary gel electrophoresis (WES, Protein Simple). The integrated peak areas of HDAC2 were divided by the integrated peak areas of SOD1 to correct for potential variation in total protein content. The vehicle condition (DMSO) was used as the reference for fold-change calculations for the different compound concentration conditions at the respective temperature. pEC_{50} values were calculated as described above.

Nano differential scanning fluorimetry with recombinant DHRS1. His-Flag tagged recombinant DHRS1 (amino acids 3–262) was expressed in *E. coli* (strain) and purified via Ni-NTA to a purity of 90%. Thermal-shift assays were performed using the Prometheus NT.48 (Nano Temper technologies) according to the manufacturer's instructions. Panobinostat or its metabolites at 100 μM were added to recombinant DHRS1 at 100 $\mu\text{g ml}^{-1}$ and analyzed using a temperature range of 20 – 90°C with a temperature slope of $1.0^\circ\text{C min}^{-1}$. The T_m was determined as the first derivative of the fluorescence ratio of 350 nm to 330 nm. All experiments were performed in duplicate. A T_m could not be determined for metabolites with autofluorescence.

Untargeted metabolomics analysis of rat spleen slices treated ex vivo with panobinostat. Fresh rat spleen tissue punches were prepared as described above. Spleen punches were treated for 1 h at 37°C with different concentrations of panobinostat or vehicle as indicated, in DMEM high glucose (Gibco), supplemented with 10% FBS, penicillin–streptomycin 100 U ml^{-1} (Gibco), L-glutamine 4.5 g l^{-1} and 10 mM HEPES (Gibco). The tissue punches were rinsed with buffer (75 mM ammonium carbonate dissolved in deionized water, pH adjusted to 7.4 with acetic acid), snap frozen in liquid nitrogen and stored at -80°C . Frozen tissue slices were mixed with $5 \mu\text{g ml}^{-1}$ of deionized water and disrupted by bead ruptor as described above. Subsequently, 50 μl of homogenates were transferred to 1.5-ml tubes and mixed with 1 ml of a 70:30 (vol/vol) ethanol:water solution heated to 75°C . Samples were incubated at 75°C for 2 min with occasional vortexing, placed on ice for 10 min and centrifuged at 13,000g for 10 min to pellet debris. Supernatants were vacuum dried as described above and finally reconstituted in 100 μl of deionized water. To enable quantification of panobinostat and its four metabolites M37.8, M43.5, M36.9 and T27C, defined concentrations of the four compounds were added to spleen lysate before homogenization. Calibration curve samples were subsequently processed identically to the remaining spleen samples to ensure data comparability. Samples were analyzed on a LC–MS platform consisting of a Thermo Scientific Ultimate 3000 liquid chromatography system with autosampler temperature set to 10°C coupled to a Thermo Scientific Q-Exactive Plus Fourier transform mass spectrometer equipped with a heated electrospray ion source and operated in negative-ionization mode. The isocratic flow rate was $150 \mu\text{l min}^{-1}$ of mobile phase consisting of 60:40 (vol/vol) isopropanol:water buffered with 1 mM ammonium fluoride, pH 9 and containing 10 nM taurocholic acid and 20 nM homotaurine as lock masses. Mass spectra were recorded in profile mode from m/z of 50 to 1,000 with the following instrument settings: sheath gas, 35 a.u. (arbitrary units); auxiliary gas, 10 a.u.; auxiliary gas heater, 200°C ; sweep gas, 1 a.u.; spray voltage, -3 kV ; capillary temperature, 250°C ; S-lens RF level, 50 a.u.; resolution, 70,000 at an m/z of 2,000; AGC target, 3×10^6 ions; maximum injection time, 120 ms; acquisition duration, 60 s. Spectral data processing was performed using an automated pipeline in R as described previously⁴¹. Detected ions were tentatively annotated as metabolites using the HMDB database⁴² as reference assuming [M–H][–] and [M–2H][–] as ionization options and the exchange of one or two ^{12}C with the equivalent number of ^{13}C atoms, with the method-inherent disability to distinguish between isomers. The full dataset

of \log_{10} -transformed ion intensities in all samples is available as Supplementary Data 14, metabolite annotation details are provided as Supplementary Data 13 and additional information on panobinostat and its metabolites relevant for this study are provided as Supplementary Data 15.

Panobinostat metabolisation in rat liver S9 and thermal shift assay. Male Wistar rat liver S9 (BioIVT, M00022) at a protein concentration of 2 mg ml^{-1} were incubated for 2 h at 37°C in the presence of 100 μM panobinostat or DMSO and a co-factor mix consisting of 1 mM nicotinamide adenine dinucleotide phosphate (NADP, Roche, 10128058001), 0.5 mM uridine 5'-diphosphoglucuronic acid (UDPGA, Sigma, U6751), 0.05 mg ml^{-1} adenosine 3'-phosphate 5'-phosphosulfate (PAPS, Sigma, A1651) and 0.05 mM L-glutathione (GSH, Sigma, G4251). Wells of a PCR plate were filled with 100 μl (each) of each reaction. Samples were heated in parallel for 3 min to 37, 47.7, 51.1, 54.2, 57.2 or 60.7°C . Heat-treated samples were then rested for 3 min at room temperature. Igepal CA-630 (I3021) was added to a concentration of 0.8%, MgCl_2 (M1028) to 1.5 mM and benzonase to 1 kU ml^{-1} , and samples were incubated for 1 h at 4°C . Aggregated proteins were separated by ultracentrifugation (20 min, 100,000g). Samples were further processed for LC–MS/MS analysis.

Synthesis of panobinostat metabolites. Unless otherwise stated, all solvents and chemicals like the building blocks were used as purchased without further purification. Preparative high-performance liquid chromatography (HPLC) was performed on a Waters autopurification system (2767 sample manager, 2545 binary gradient module, 2420 ELS detector, 2996 photodiode array detector, 3100 mass detector, Waters SFO, and Waters 515 HPLC pump). The purification was done on a Xbridge BEH C18 OBD 5 μm Prep Column using a water–acetonitrile mixture (0.2% formic acid as modifier) at a flow rate of 30 ml min^{-1} . The purity of all test compounds was 95% or higher as determined by analytical ultra-performance liquid chromatography was done on a Waters Acquity BEH C18 1.7 μm column (2.1 \times 50 mm) at 40°C and a flow rate of 0.5 ml min^{-1} with a linear gradient over 1 min (5–100% acetonitrile in water, 0.2% formic acid as modifier). The instrument used for analysis was a waters Acquity system (detectors: Acquity SQD and Acquity PDA). Mass signals were determined using a Waters 3100 mass detector. Alternatively for synthesis of (2S,3S,4S,5S,6S)-3,4,5-trihydroxy-6-(((E)-3-(4-(((2-(2-methyl-1H-indol-3-yl)ethyl)amino)methyl)phenyl)acrylamido)oxy)tetrahydro-2H-pyran-2-carboxylic acid the purity was determined using an Agilent 1290 Infinity II and mass signals were determined by MSD 6130. The column was Sunfire C-18 (30 \times 2.1 mm) 3.5 μm and a flow rate of 1.0 ml min^{-1} with a linear gradient over 3 min (0–100% acetonitrile in water, 0.1% formic acid as modifier). (1H) NMR spectra were recorded on a Bruker Avance 400 spectrometer (400 MHz) using DMSO- d_6 as solvent. Chemical shifts are given in p.p.m. (δ relative to residual solvent peak for 1H).

4-(((2-(2-Methyl-1H-indol-3-yl)ethyl)amino)methyl)benzoic acid (M36.9). 2-(2-Methyl-1H-indol-3-yl)ethan-1-amine (50 mg, 0.287 mmol) was dissolved in ethanol (0.5 ml) and to this solution was added 4-formylbenzoic acid (64.6 mg, 0.430 mmol) followed by sodium cyanoborohydride (36.1 mg, 0.574 mmol). The reaction mixture was stirred overnight at room temperature and then diluted with 5% NaHSO_4 (aq.) (10 ml). This was then extracted with ethyl acetate (2 \times 10 ml) and the organic phase was dried over sodium sulfate, filtered and evaporated. The residue was purified by preparatory HPLC. This afforded 4-(((2-(2-methyl-1H-indol-3-yl)ethyl)amino)methyl)benzoic acid (17 mg, 0.054 mmol, 18.83% yield) as a white solid. LC–MS m/z 307.3 [M–H][–] (Rt = 0.72 min). ¹H NMR (DMSO- d_6 , 400 MHz) δ 12.07 (br s, 1H), 7.6–7.6 (m, 3H), 7.35 (t, 2H, $J = 7.7 \text{ Hz}$), 7.2–7.3 (m, 1H), 7.07 (d, 1H, $J = 1.3 \text{ Hz}$), 6.85 (s, 1H), 4.0–4.2 (m, 4H), 3.61 (s, 2H), 2.26 (s, 3H). (E)-3-(4-(((2-(2-Methyl-1H-indol-3-yl)ethyl)amino)methyl)phenyl)acrylamide (37.8) was synthesized as previously described⁴.

(E)-3-(4-(((2-(2-Methyl-1H-indol-3-yl)ethyl)amino)methyl)phenyl)acrylic acid (M43.5). Methyl (E)-3-(4-(((2-(2-methyl-1H-indol-3-yl)ethyl)amino)methyl)phenyl)acrylate (30 mg, 0.086 mmol) was dissolved in tetrahydrofuran (0.4 ml) and to this was added an aqueous solution of NaOH (1 M, 0.1 ml). The reaction mixture was then stirred overnight and then 5% NaHSO_4 (aq) was added. The precipitate was collected by filtration and was washed with water and ethyl acetate. This afforded (E)-3-(4-(((2-(2-methyl-1H-indol-3-yl)ethyl)amino)methyl)phenyl)acrylic acid (9 mg, 0.027 mmol, 31.3% yield) as a white solid. LC–MS m/z 333.3 [M–H][–] (Rt = 0.74 min). ¹H NMR (DMSO- d_6 , 400 MHz) δ 10.80 (s, 1H), 7.71 (d, 2H, $J = 8.1 \text{ Hz}$), 7.59 (d, 1H, $J = 16.1 \text{ Hz}$), 7.47 (d, 2H, $J = 8.1 \text{ Hz}$), 7.39 (d, 1H, $J = 7.6 \text{ Hz}$), 7.24 (d, 1H, $J = 7.9 \text{ Hz}$), 6.9–7.0 (m, 2H), 6.56 (d, 1H, $J = 16.1 \text{ Hz}$), 4.04 (s, 2H), 2.90 (s, 4H), 2.32 (s, 3H).

N-Hydroxy-3-(4-(((2-(2-methyl-1H-indol-3-yl)ethyl)amino)methyl)phenyl)propanamide (T27c). 3-(4-(((2-(2-Methyl-1H-indol-3-yl)ethyl)amino)methyl)phenyl)propanoic acid (63 mg, 0.187 mmol) was dissolved in *N,N*-dimethylformamide (1 ml) and to this was added *O*-(*tert*-butyl)hydroxylamine (83 mg, 0.936 mmol), DIPEA (0.196 ml, 1.124 mmol) and finally HATU (107 mg, 0.281 mmol). The reaction mixture was then stirred for 18 h at room temperature and then purified directly by reverse phase column chromatography eluting with

acetonitrile in water (10–80%). This afforded *N*-(*tert*-butoxy)-3-(4-(((2-(2-methyl-1*H*-indol-3-yl)ethyl)amino)methyl)phenyl) propanamide (19 mg, 0.047 mmol, 24.90% yield) as a colorless solid. LC–MS *m/z* 408.3 [M + H]⁺ (Rt = 0.80 min).

N-(*tert*-Butoxy)-3-(4-(((2-(2-methyl-1*H*-indol-3-yl)ethyl)amino)methyl)phenyl)propanamide (19 mg, 0.047 mmol) was dissolved in dichloromethane (0.2 ml) and to this was added trifluoroacetic acid (0.3 ml, 3.89 mmol). The reaction mixture was stirred at room temperature for 5 h. The solvent was then removed in vacuo and the residue was purified by preparatory HPLC. This afforded *N*-hydroxy-3-(4-(((2-(2-methyl-1*H*-indol-3-yl)ethyl)amino)methyl)phenyl)propanamide (9 mg, 0.026 mmol, 54.9 % yield) as a colorless solid. LC–MS *m/z* 352.2 [M + H]⁺ (Rt = 0.70 min). ¹H NMR (DMSO-*d*₆, 400 MHz) δ 10.74 (s, 1H), 10.39 (s, 1H), 8.27 (s, 1H), 7.38 (d, 1H, *J* = 7.6 Hz), 7.1–7.3 (m, 5H), 6.8–7.0 (m, 2H), 3.80 (s, 2H), 2.7–2.9 (m, 6H), 2.31 (s, 3H), 2.2–2.3 (m, 2H).

3-(4-(((2-(2-Methyl-1*H*-indol-3-yl)ethyl)amino)methyl)phenyl)propanoic acid (M44.6). 2-(2-Methyl-1*H*-indol-3-yl)ethan-1-amine (200 mg, 1.148 mmol) was dissolved in ethanol (2 mL) and to this was added 3-(4-formylphenyl)propanoic acid (307 mg, 1.722 mmol), followed by sodium cyanoborohydride (144 mg, 2.296 mmol). The reaction mixture was then stirred at room temperature for 18 h. It was then diluted with 5% NaHSO₄(aq) (10 mL) and extracted with ethyl acetate (2 × 20 mL). The combined organic phases were dried over sodium sulfate, filtered and evaporated. The residue was purified by reverse phase column chromatography eluting with acetonitrile in water (0 to 100 % containing 0.2% formic acid). The product was further purified by dissolving it in ethyl acetate (20 mL) and washing with 0.5 M HCl (2 × 20 mL). The organic phase was dried over sodium sulfate, filtered and evaporated. The residue was finally purified by reverse phase chromatography eluting with acetonitrile in water (10–100% containing 1% ammonia). This afforded 3-(4-(((2-(2-methyl-1*H*-indol-3-yl)ethyl)amino)methyl)phenyl)propanoic acid (20 mg, 0.059 mmol, 5.13 % yield) as a white solid. MS *m/z* 337.3 [M + H]⁺ (Rt = 0.77 min). ¹H NMR (DMSO-*d*₆, 400 MHz) δ 10.63 (s, 1H), 7.3 (d, 1H, *J* = 7.7), 7.20–7.25 (m, 3H), 7.15 (d, 2H, *J* = 8.4), 6.8–6.9 (m, 1H), 6.75–6.8 (m, 1H), 3.69 (s, 2H), 2.7–2.8 (m, 4H), 2.6–2.7 (m, 2H), 2.3–2.4 (m, 2H), 2.23 (s, 3H).

3-(4-(((2-(5-Hydroxy-2-methyl-1*H*-indol-3-yl)ethyl)amino)methyl)phenyl)propanoic acid (T25g). 3-(2-Aminoethyl)-2-methyl-1*H*-indol-5-ol (25 mg, 0.131 mmol) was dissolved in ethanol (0.5 ml) and to this was added 3-(4-formylphenyl)propanoic acid (25.8 mg, 0.145 mmol) followed by sodium cyanoborohydride (12.39 mg, 0.197 mmol). The reaction mixture was then stirred at room temperature overnight. The solvent was removed in vacuo and the residue was purified by reverse-phase column chromatography eluting with acetonitrile in water (0–100% containing 0.2% formic acid). This afforded 3-(4-(((2-(5-hydroxy-2-methyl-1*H*-indol-3-yl)ethyl)amino)methyl)phenyl)propanoic acid, formic acid salt (5 mg, 0.012 mmol, 9.4% yield) as a white solid. Mass spectrometry *m/z* of 353.2 [M + H]⁺ (Rt = 0.68 min). ¹H NMR (DMSO-*d*₆, 400 MHz) δ 10.38 (s, 1H), 7.2–7.3 (m, 2H), 7.1–7.2 (m, 4H), 6.92 (d, 1H, *J* = 8.5 Hz), 6.63 (d, 1H, *J* = 2.1 Hz), 6.41 (dd, 1H, *J* = 2.1, 8.5 Hz), 4.35 (s, 1H), 3.92 (br s, 2H), 2.7–2.8 (m, 6H), 2.4–2.5 (m, 2H), 2.17 (s, 3H).

(2*S*,3*S*,4*S*,5*S*,6*S*)-3,4,5-Trihydroxy-6-(((*E*)-3-(4-(((2-(2-methyl-1*H*-indol-3-yl)ethyl)amino)methyl)phenyl)acrylamido)oxy)tetrahydro-2*H*-pyran-2-carboxylic acid (M34.4). To a solution of methyl (*E*)-3-(4-(((2-(2-methyl-1*H*-indol-3-yl)ethyl)amino)methyl)phenyl)acrylate (4 g, 11.48 mmol) in 1,4-dioxane (50 ml) and water (5 ml) at 0 °C was added triethylamine (4.80 ml, 34.4 mmol), followed by Boc-anhydride (8.00 ml, 34.4 mmol). The reaction mixture was stirred at 25 °C for 48 h and then the solvent was evaporated in vacuo. The residue was partitioned between ethyl acetate (100 ml) and water (100 ml). The organic phase was washed with saturated brine (50 ml), dried over sodium sulfate and evaporated in vacuo to afford (*E*)-3-(4-(((*tert*-butoxycarbonyl)(2-(2-methyl-1*H*-indol-3-yl)ethyl)amino)methyl)phenyl)acrylate (5.0 g, 92% yield) as a brown oil. Mass spectrometry *m/z* of 393.2 [M(-tBu) + H]⁺ (Rt = 2.82 min).

A solution of methyl (*E*)-3-(4-(((*tert*-butoxycarbonyl)(2-(2-methyl-1*H*-indol-3-yl)ethyl)amino)methyl)phenyl)acrylate (5 g, 11.15 mmol) in tetrahydrofuran (50 ml) and methanol (5 ml) was cooled to 0 °C and a solution of lithium hydroxide (0.534 g, 22.29 mmol) in water (5 mL) was added. The reaction mixture was stirred at room temperature for 16 h then diluted with water (150 ml) and cooled to 0 °C. The solution was neutralized with 1.5 M HCl solution and extracted with ethyl acetate (2 × 150 ml). The combined organic layers were washed with brine (100 ml) and dried over anhydrous sodium sulfate, filtered and concentrated under reduced pressure. The residue was washed with ether (2 × 50 ml) and this afforded (*E*)-3-(4-(((*tert*-butoxycarbonyl)(2-(2-methyl-1*H*-indol-3-yl)ethyl)amino)methyl)phenyl)acrylic acid (3.9 g, 79% yield) as a white solid. Mass spectrometry *m/z* of 435.1 [M + H]⁺ (Rt = 2.49 min).

To a solution of (*E*)-3-(4-(((*tert*-butoxycarbonyl)(2-(2-methyl-1*H*-indol-3-yl)ethyl)amino)methyl)phenyl)acrylic acid (1.368 g, 3.15 mmol) in DMF (15 ml), stirred under nitrogen at 0 °C, were added HATU (1.437 g, 3.78 mmol), DIPEA (1.100 ml, 6.30 mmol) and a solution of (2*S*,3*R*,4*S*,5*S*,6*S*)-2-(aminooxy)-6-(methoxycarbonyl)tetrahydro-2*H*-pyran-3,4,5-triyl triacetate (1.1 g, 3.15 mmol) in DMF (5 ml) dropwise. The reaction mixture was stirred at 25 °C for 5 h and then concentrated in vacuo and the residue was partitioned between ethyl acetate (80 ml) and water (60 ml). The

organic phase was washed with saturated brine (30 ml), dried over sodium sulfate and evaporated in vacuo to give the crude product. The residue was purified by column chromatography eluting with ethyl acetate in petroleum ether (0–100%) to afford (2*S*,3*R*,4*S*,5*S*,6*S*)-2-(((*E*)-3-(4-(((*tert*-butoxycarbonyl)(2-(2-methyl-1*H*-indol-3-yl)ethyl)amino)methyl)phenyl)acrylamido)oxy)-6-(methoxycarbonyl)tetrahydro-2*H*-pyran-3,4,5-triyl triacetate (1.1 g, 39.2% yield) as a pale yellow solid. Mass spectrometry *m/z* of 766.3 [M + H]⁺ (Rt = 2.62 min).

To a solution of (2*S*,3*R*,4*S*,5*S*,6*S*)-2-(((*E*)-3-(4-(((*tert*-butoxycarbonyl)(2-(2-methyl-1*H*-indol-3-yl)ethyl)amino)methyl)phenyl)acrylamido)oxy)-6-(methoxycarbonyl)tetrahydro-2*H*-pyran-3,4,5-triyl triacetate (900 mg, 1.175 mmol) in 1,4-dioxane (10 ml), stirred under nitrogen at 0 °C, was added hydrochloric acid (4.5 M) in dioxane (5 ml, 22.50 mmol) dropwise. The reaction mixture was stirred at 25 °C for 3 h and then was concentrated under reduced pressure, diluted with water (50 ml), neutralized with 15% NaHCO₃ solution and extracted with ethyl acetate (2 × 60 ml). The organic phase was washed with saturated brine (50 ml), dried over sodium sulfate and evaporated in vacuo. The crude compound was washed with ether (2 × 10 ml) and dried under reduced pressure to afford (2*S*,3*S*,4*S*,5*R*,6*S*)-2-(methoxycarbonyl)-6-(((*E*)-3-(4-(((2-(2-methyl-1*H*-indol-3-yl)ethyl)amino)methyl)phenyl)acrylamido)oxy)tetrahydro-2*H*-pyran-3,4,5-triyl triacetate (0.6 g, 58.2% yield) as an off white solid. Mass spectrometry *m/z* of 665.9 [M + H]⁺ (Rt = 1.58 min).

To a solution of (2*S*,3*S*,4*S*,5*R*,6*S*)-2-(methoxycarbonyl)-6-(((*E*)-3-(4-(((2-(2-methyl-1*H*-indol-3-yl)ethyl)amino)methyl)phenyl)acrylamido)oxy)tetrahydro-2*H*-pyran-3,4,5-triyl triacetate (550 mg, 0.826 mmol) in methanol (10 ml) under nitrogen at –10 °C was added sodium hydroxide (2 ml, 2.000 mmol) dropwise. The reaction mixture was stirred at 0 °C for 30 min. The reaction mixture was neutralized at 0 °C with acetic acid and the solvent was removed in vacuo. The residue was purified by preparatory HPLC. This afforded (2*S*,3*S*,4*S*,5*S*,6*S*)-3,4,5-trihydroxy-6-(((*E*)-3-(4-(((2-(2-methyl-1*H*-indol-3-yl)ethyl)amino)methyl)phenyl)acrylamido)oxy)tetrahydro-2*H*-pyran-2-carboxylic acid (55 mg, 12.4% yield) as a pale yellow solid. Mass spectrometry *m/z* of 526.2 [M + H]⁺ (Rt = 1.27 min). ¹H NMR (DMSO-*d*₆, 400 MHz): δ 10.76 (s, 1H), 7.57–7.55 (m, 1H), 7.47–7.39 (m, 4H), 7.23 (d, *J* = 8.0 Hz, 1H), 6.99–6.90 (m, 2H), 6.48 (d, *J* = 15.5 Hz, 1H), 5.05 (bs, 1H), 4.61 (d, *J* = 7.2 Hz, 1H), 4.0 (s, 2H), 3.49 (d, *J* = 8.3 Hz, 1H), 3.24–3.21 (m, 3H), 3.17–3.13 (m, 2H), 2.95–2.83 (m, 4H), 2.32 (s, 3H).

Density plots. Density plots shown were generated using R and the ggplot2 package.

Box plots. Box plots shown were generated using R and the ggplot2 package. The lower and the upper hinges of the boxes correspond to the 25th and 75th percentiles, the bar in the box shows the median. The upper whisker extends from the upper hinge to the largest value (up to a maximum of 1.5 × IQR). Similarly, the lower whisker extends from the lower hinge to at most 1.5 × IQR. Points outside of the whiskers were plotted individually as outliers.

Group tests were performed using a nonparametric Wilcoxon test and statistical significance is indicated by: **P* ≤ 0.05, ***P* ≤ 0.01 and ****P* ≤ 0.001 if not stated otherwise.

Ethics statement. Human blood was sourced ethically with written informed consent and its research use was in accordance with the terms of the informed consent under an IRB/EC approved protocol (Ethics Commission at the Landesärztekammer Baden-Wuerttemberg, Germany). The animal experiments were ethically reviewed by the GSK Office for Animal Welfare, Ethics and Strategy and carried out in accordance with European Directive 2010/63/EEC and the GSK Policy on the Care, Welfare and Treatment of Animals.

Reporting Summary. Further information on research design is available in the Nature Research Reporting Summary linked to this article.

Data availability

All data is available in the main text or the supplementary materials. The mass spectrometry proteomics data have been deposited to the ProteomeXchange Consortium via the PRIDE²⁴ partner repository with the dataset identifiers PXD015458, PXD015427, PXD015397, PXD015373 and PXD016277.

Code availability

The code used for this study will be made available by the corresponding authors upon reasonable request.

References

- Perez-Riverol, Y. et al. The PRIDE database and related tools and resources in 2019: improving support for quantification data. *Nucleic Acids Res.* **47**, D442–D450 (2019).
- Franken, H. et al. Thermal proteome profiling for unbiased identification of direct and indirect drug targets using multiplexed quantitative mass spectrometry. *Nat. Protoc.* **10**, 1567–1593 (2015).

26. Density and mass of each organ/tissue *Bionumbers* <http://kirschner.med.harvard.edu/files/bionumbers/Density%20and%20mass%20of%20each%20organ-tissue.pdf> (2014).
27. Moggridge, S., Sorensen, P. H., Morin, G. B. & Hughes, C. S. Extending the compatibility of the SP3 paramagnetic bead processing approach for proteomics. *J. Proteome Res.* **17**, 1730–1740 (2018).
28. Kelstrup, C. D. et al. Limits for resolving isobaric tandem mass tag reporter ions using phase-constrained spectrum deconvolution. *J. Proteome Res.* **17**, 4008–4016 (2018).
29. Werner, T. et al. Ion coalescence of neutron encoded TMT 10-plex reporter ions. *Anal. Chem.* **86**, 3594–3601 (2014).
30. Savitski, M. M. et al. Measuring and managing ratio compression for accurate iTRAQ/TMT quantification. *J. Proteome Res.* **12**, 3586–3598 (2013).
31. Savitski, M. M. et al. Targeted data acquisition for improved reproducibility and robustness of proteomic mass spectrometry assays. *J. Am. Soc. Mass Spectrom.* **21**, 1668–1679 (2010).
32. Poole, W., Gibbs, D. L., Shmulevich, I., Bernard, B. & Knijnenburg, T. A. Combining dependent *P*-values with an empirical adaptation of Brown's method. *Bioinformatics* **32**, i430–i436 (2016).
33. Benjamini, Y. & Hochberg, Y. Controlling the false discovery rate: a practical and powerful approach to multiple testing. *J. R. Stat. Soc. Ser. B Methodol* **57**, 289–300 (1995).
34. Silva, J. C., Gorenstein, M. V., Li, G.-Z., Vissers, J. P. C. & Geromanos, S. J. Absolute quantification of proteins by LCMSE: a virtue of parallel MS acquisition. *Mol. Cell. Proteomics* **5**, 144–156 (2006).
35. Eden, E., Navon, R., Steinfeld, I., Lipson, D. & Yakhini, Z. GORilla: a tool for discovery and visualization of enriched GO terms in ranked gene lists. *BMC Bioinformatics* **10**, 48 (2009).
36. Eden, E., Lipson, D., Yogev, S. & Yakhini, Z. Discovering motifs in ranked lists of DNA sequences. *PLoS Comput. Biol.* **3**, e39 (2007).
37. Ruepp, A. et al. CORUM: the comprehensive resource of mammalian protein complexes. *Nucleic Acids Res.* **36**, D646–D650 (2008).
38. Ruepp, A. et al. CORUM: the comprehensive resource of mammalian protein complexes—2009. *Nucleic Acids Res.* **38**, D497–D501 (2010).
39. Vinayagam, A. et al. Protein complex-based analysis framework for high-throughput data sets. *Sci. Signal.* **6**, rs5 (2013).
40. Ori, A. et al. Spatiotemporal variation of mammalian protein complex stoichiometries. *Genome Biol.* **17**, 47 (2016).
41. Fuhrer, T., Heer, D., Begemann, B. & Zamboni, N. High-throughput, accurate mass metabolome profiling of cellular extracts by flow injection-time-of-flight mass spectrometry. *Anal. Chem.* **83**, 7074–7080 (2011).
42. Wishart, D. S. et al. HMDB 4.0: the human metabolome database for 2018. *Nucleic Acids Res.* **46**, D608–D617 (2018).

Acknowledgements

The authors thank J. Stuhlfauth, N. Garcia-Altrieth, L. Vitali, K. Beß and B. Dlugosch for the supporting cell culture and lysate production; M. Bösch, T. Rudi, M. Klös-Hudak, K. Kammerer and M. Steidel for assistance with mass spectrometry; A. Wolf for supporting the DSF assay; S. Gade for support during data uploading; C. Schofield, T. Walker, G. Drewes, F. Reinhard, P. Grandi and P. Wier for scientific discussions; and E. Nicodeme and F. Blandel for excellent technical support during the animal study.

Author contributions

J.P., T.W., C.E.R., E.S., K.S., J.K., B.H., I.B. and D.P. designed and performed experiments and analyzed TPP data; A.R., K.S., B.H. and T.W. designed and performed experiments and analyzed the data for whole blood; D.W.T. synthesized compounds; D.C.S. and J.V. performed and analyzed the metabolomics experiments; H.C.E. analyzed the DSF experiment; N.K., D.D.C., M.K., H.F. and M.F.-S. performed the statistical analysis; W.H. gave scientific and data analysis advice; G.B., M.B. and M.M.S. designed experiments, analyzed data and wrote the manuscript; and G.B. supervised the work.

Competing interests

J.P., T.W., A.R., D.P., E.S., K.S., B.H., D.W.T., J.K., J.V., D.C.S., H.C.E., H.F., M.F.S., M.B. and G.B. are GSK employees. M.M.S. is a GSK shareholder.

Additional information

Supplementary information is available for this paper at <https://doi.org/10.1038/s41587-019-0388-4>.

Correspondence and requests for materials should be addressed to M.M.S., M.B. or G.B.

Reprints and permissions information is available at www.nature.com/reprints.

Reporting Summary

Nature Research wishes to improve the reproducibility of the work that we publish. This form provides structure for consistency and transparency in reporting. For further information on Nature Research policies, see [Authors & Referees](#) and the [Editorial Policy Checklist](#).

Statistics

For all statistical analyses, confirm that the following items are present in the figure legend, table legend, main text, or Methods section.

n/a Confirmed

- The exact sample size (n) for each experimental group/condition, given as a discrete number and unit of measurement
- A statement on whether measurements were taken from distinct samples or whether the same sample was measured repeatedly
- The statistical test(s) used AND whether they are one- or two-sided
Only common tests should be described solely by name; describe more complex techniques in the Methods section.
- A description of all covariates tested
- A description of any assumptions or corrections, such as tests of normality and adjustment for multiple comparisons
- A full description of the statistical parameters including central tendency (e.g. means) or other basic estimates (e.g. regression coefficient) AND variation (e.g. standard deviation) or associated estimates of uncertainty (e.g. confidence intervals)
- For null hypothesis testing, the test statistic (e.g. F , t , r) with confidence intervals, effect sizes, degrees of freedom and P value noted
Give P values as exact values whenever suitable.
- For Bayesian analysis, information on the choice of priors and Markov chain Monte Carlo settings
- For hierarchical and complex designs, identification of the appropriate level for tests and full reporting of outcomes
- Estimates of effect sizes (e.g. Cohen's d , Pearson's r), indicating how they were calculated

Our web collection on [statistics for biologists](#) contains articles on many of the points above.

Software and code

Policy information about [availability of computer code](#)

Data collection

The mass spectrometers Q Exactive Orbitrap and Orbitrap Fusion Lu mos (Thermo Fischer Scientific) were used for data acquisition and the instruments were operated with Tune 2.2 or 2.3 and Xcalibur 2.7 or 3.0.63

Data analysis

Mascot 2.4 (Matrix Science) was used for peptide searching; isobarQuant (<https://github.com/protcode/isob/archive/1.1.0.zip>) was used to quantify peptide and protein abundances; proteins were searched using Uniprot or Swissprot; R 3.5.1 was used for custom data analysis; the R ggplot2 package 3.0.0 was used to generate the densityplots, scatterplots and the boxplots; heatmaps were generated with the R packages pheatmap and ComplexHeatmap; the enrichment webtool Gorilla webtool was used for the gene ontology enrichment; Tibco Spotfire 7.0.1.24 was used for clustering; GraphPad Prism 7 was used to fit and display dose response curves.

For manuscripts utilizing custom algorithms or software that are central to the research but not yet described in published literature, software must be made available to editors/reviewers. We strongly encourage code deposition in a community repository (e.g. GitHub). See the Nature Research [guidelines for submitting code & software](#) for further information.

Data

Policy information about [availability of data](#)

All manuscripts must include a [data availability statement](#). This statement should provide the following information, where applicable:

- Accession codes, unique identifiers, or web links for publicly available datasets
- A list of figures that have associated raw data
- A description of any restrictions on data availability

All data is available in the main text or the supplementary materials. The mass spectrometry proteomics data have been deposited to the ProteomeXchange Consortium via the PRIDE partner repository with the dataset identifiers PXD015458, PXD015427, PXD015397, PXD015373 and PXD016277.

Field-specific reporting

Please select the one below that is the best fit for your research. If you are not sure, read the appropriate sections before making your selection.

Life sciences Behavioural & social sciences Ecological, evolutionary & environmental sciences

For a reference copy of the document with all sections, see [nature.com/documents/nr-reporting-summary-flat.pdf](https://www.nature.com/documents/nr-reporting-summary-flat.pdf)

Life sciences study design

All studies must disclose on these points even when the disclosure is negative.

Sample size	Biological triplicates have been used for all in vivo data sets to gain appropriate power for discovery of true positive events. Biological duplicates or more were used for all in vitro data sets. Details on sample size for experiments were indicated in methods and figure legends.
Data exclusions	No data were excluded from the analyses
Replication	Conclusions were drawn from reproducible effects in all triplicates for the in vivo data sets and from reproducible effects in duplicates for all in vitro data sets
Randomization	Rats for the in vivo study were randomly distributed into the 2 treatment groups
Blinding	The investigators were not blinded to the treatment conditions since this information had to be used for statistical analysis.

Reporting for specific materials, systems and methods

We require information from authors about some types of materials, experimental systems and methods used in many studies. Here, indicate whether each material, system or method listed is relevant to your study. If you are not sure if a list item applies to your research, read the appropriate section before selecting a response.

Materials & experimental systems

Methods

n/a	Involved in the study
<input type="checkbox"/>	<input checked="" type="checkbox"/> Antibodies
<input type="checkbox"/>	<input checked="" type="checkbox"/> Eukaryotic cell lines
<input checked="" type="checkbox"/>	<input type="checkbox"/> Palaeontology
<input type="checkbox"/>	<input checked="" type="checkbox"/> Animals and other organisms
<input type="checkbox"/>	<input checked="" type="checkbox"/> Human research participants
<input checked="" type="checkbox"/>	<input type="checkbox"/> Clinical data

n/a	Involved in the study
<input checked="" type="checkbox"/>	<input type="checkbox"/> ChIP-seq
<input checked="" type="checkbox"/>	<input type="checkbox"/> Flow cytometry
<input checked="" type="checkbox"/>	<input type="checkbox"/> MRI-based neuroimaging

Antibodies

Antibodies used	Anti-phospho-STAT5a/b (Ser726, Ser731), Invitrogen, cat: PA5-36767; Anti-total STAT5b, Invitrogen, cat: 135300; Anti-HDAC2, Cell Signaling Technology, cat: 5113; anti-HDAC2, Abcam, cat: Ab124974; Anti-SOD1, Novus; Anti-DHRS1, Sigma-Aldrich, cat: HPA000599.
Validation	The antibodies listed above have been used for westernblot analysis (anti-phospho-STAT5a/b, anti-STAT5b, anti-DHRS1) or for capillary gel electrophoresis (anti-HDAC2, anti-SOD1). All antibodies detected a band at the expected molecular weight in the experiments reported in this manuscript and also detected a band at the expected molecular on the respective datasheet from the providers.

Eukaryotic cell lines

Policy information about [cell lines](#)

Cell line source(s)	RBL-2H3 cells and HL-60 cells were from DSMZ. HepG2 cells and THP-1 cells were from ATCC.
Authentication	Authenticated using Promega kit
Mycoplasma contamination	Confirmed negative in check for mycoplasma contamination
Commonly misidentified lines (See ICLAC register)	To the best of our knowledge no misidentified cell lines have been used in this study.

Animals and other organisms

Policy information about [studies involving animals](#); [ARRIVE guidelines](#) recommended for reporting animal research

Laboratory animals	10 weeks old male Han Wistar rats (CrI: WI(Han)) were used for in the study.
Wild animals	The study did not involve wild animals.
Field-collected samples	The study did not involve samples collected from the field.
Ethics oversight	The animal experiments were ethically reviewed and carried out in accordance with European Directive 2010/63/EEC and the GSK Policy on the Care, Welfare and Treatment of Animals.

Note that full information on the approval of the study protocol must also be provided in the manuscript.

Human research participants

Policy information about [studies involving human research participants](#)

Population characteristics	PBMCs were isolated from blood donated by healthy volunteers (of any gender and age) with written informed consent.
Recruitment	Blood was obtained from healthy volunteers at the Heidelberg blood center (Institut für Klinische Transfusionsmedizin und Zelltherapie gGmbH) or from the internal donor panel (Cellzome GmbH, Heidelberg).
Ethics oversight	Human blood was sourced ethically and its research use was in accordance with the terms of the informed consent under an IRB/EC approved protocol (Ethics Commission at the Landesärztekammer Baden-Wuerttemberg, Germany).

Note that full information on the approval of the study protocol must also be provided in the manuscript.